A STUDY OF MEAN PRESSURE GRADIENTS, MEAN CAVITY PRESSURES, AND RESULTING RESIDUAL MEAN PRESSURES ACROSS A RAINSCREEN FOR A REPRESENTATIVE BUILDING

By

P.F. Skerlj and D. Surry
Boundary Layer Wind Tunnel Laboratory
September 1994

Presented to:

Jacques Rousseau and Pierre-Michel Busque
Housing Innovation Division

NOTE: **DISPONIBLE AUSSI *EN* FRANÇAIS SOUS LE TITRE:**

ÉTUDE SUR LES GRADIENTS DE PRESSION MOYENNE, LES PRESSIONS MOYENNES DES CAVITÉS ET LES PRESSIONS MOYENNES RÉSIDUELLES EXERCÉES SUR LES ÉCRANS PARE-PLUIE D'UN BÂTIMENT REPRÉSENTATIF

This report has been approved by:

Dr. A.G. Davenport
Director

Boundary Layer Wind Tunnel Laboratory
The Faculty of Engineering Science
The University of Western Ontario
London, Ontario, Canada N6A 5B9

Tel: 519-661-3338
Fax: 519-661-3339

CMHC MANDATE

Canada Mortgage and Housing Corporation, the Federal Government's housing agency, is responsible for administering the National Housing Act.

This legislation is designed to aid in the improvement of housing and living conditions in Canada. As a result, the Corporation has interests in all aspects of housing and urban growth and development.

Under Part IX of this Act, the Government of Canada provides funds to CMHC to conduct research into the social, economic and technical aspects of housing and related fields, and to undertake the publishing and distribution of the results of this research. CMHC therefore has a statutory responsibility to make available, information which may be useful in the improvement of housing and living conditions.

This publication is one of the many items of information published by CMHC with the assistance of federal funds.

DISCLAIMER

This study was conducted for Canada Mortgage and Housing Corporation under Part IX of the National Housing Act. The analysis, interpretation and recommendations are those of the consultants and do not necessarily reflect the views of Canada Mortgage and Housing Corporation or those divisions of the Corporation that assisted in the study and its publication.

TABLE OF CONTENTS

ACKNOWLEDGEMENTS	**1**
EXECUTIVE SUMMARY	**2**
1.0 INTRODUCTION	**3**
2.0 DESCRIPTION OF EXPERIMENTS	**4**
2.1 Compartmentalized Pressure Module	4
2.2 Building Model	4
2.3 Modelling of the Wind	5
2.4 Experimental Procedure	5
3.0 DISCUSSION OF RESULTS	**6**
REFERENCES	**12**
FIGURES	**13**
APPENDIX 1- COMPARISON OF LOSSES THROUGH VENTS TO LOSSES THROUGH TUBING	**18**
APPENDIX 2- EXPERIMENTAL RESULTS	**22**

ACKNOWLEDGEMENTS

This study was initiated by Canada Mortgage and Housing Corporation. Discussions with Jacques Rousseau and Pierre Busque were very helpful in defining the scope of the study, and their input throughout the project was greatly appreciated.

The financial contributions of both Canada Mortgage and Housing Corporation and the Natural Sciences and Engineering Research Council of Canada are acknowledged.

The authors would also like to acknowledge the contributions made by members of the Laboratory staff: Mr. D. Garnham who constructed the pressure module and building model and both Mr. S. Norman and Mr. G. Dafoe who assisted in initial phases of the experiment.

EXECUTIVE SUMMARY

Experiments were conducted in the Boundary Layer Wind Tunnel at the University of Western Ontario to investigate the equalization of mean pressures occurring in rainscreen walls.

Canada Mortgage and Housing Corporation, through their interest in wind, rain and the building envelope, initiated this project. In particular, Jacques Rousseau aided in the development of the scope of this study through discussions with Alan Davenport and David Surry of the BLWTL. The objectives were to examine the mean pressure gradients on the external surface of a representative building and to investigate the resulting net rainscreen pressures.

A module comprising a variable number of vented compartments was used to determine external mean pressure distributions, mean cavity pressures and resulting mean pressures across the outer wall of a rectangular building model at six locations on the long face (see Figure 2). At each location, wind angles ranging from normal to parallel to the long building face were examined. The bulk of experiments were performed using a compartment width (the dimension parallel to the array of external pressure taps) of 2 m in full scale. A limited number of experiments were also performed which considered 1 m, 2 m, 4 m and 8 m compartment widths.

External pressure results show steep horizontal and vertical external mean pressure gradients near side and top edges respectively. For a typical 10 year dynamic pressure of 300 Pa (hourly mean speed of 78 km/hr), pressure gradients as large as 260 Pa/m were measured near the top corner. The gradients over interior regions of the building face were generally found to be smaller.

Measurements of mean internal cavity pressures verify that compartments do not pressure equalize when exposed to large external gradients. In this situation, significant residual mean pressure differences result across the rainscreen (see, for example, Table 2).

As expected, net mean rainscreen pressures were found to decrease with decreasing compartment size and with decreasing mean pressure gradient. Hence, regions near edges, which generally contain large external pressure gradients, require frequent compartmentalization to reduce residual pressures.

1.0 INTRODUCTION

A pressure-equalized rainscreen wall consists of an outer wall (the rainscreen) and an inner wall, separated by an air space (the cavity). The inner wall performs numerous functions, one of which is to act as an air barrier that prevents air movement between the outdoors and the interior of the building. The rainscreen contains small protected openings to vent the cavity with the outside in a bid to balance the pressures on either side. This wall design is intended to prevent rain penetration via wind-induced air-pressure differentials.

If the external pressure is spatially uniform and does not vary with time and the air barrier is well sealed, there should be no pressure difference across the rainscreen. Violations to any of these three conditions will lead to some pressure difference across the rainscreen. In this report, interest is focussed on the mean pressure situation (neglecting time variations) where the air barrier is well sealed, but where mean pressure gradients occur over the outer surface. Clearly, if the cavity is subdivided into small enough compartments with each being independently vented, then the change in external pressure over any single compartment can be made arbitrarily small.

This work was undertaken to examine the severity of the mean pressure gradients that exist on the external surface of a representative building and to verify that mean cavity pressures follow the simple theoretical models in the literature.

Mean pressure experiments were conducted in the Boundary Layer Wind Tunnel Laboratory at the University of Western Ontario. A compartmentalized pressure module was designed to investigate mean pressure equalization of rainscreen cladding under the influence of external mean pressure gradients. The pressure module was capable of being located anywhere on the building model. A row of external pressure taps was used to obtain external mean pressure distributions, and internal taps defined mean cavity pressures. The design allowed the number and size of compartments along the array of external pressure taps to be easily altered.

This report first describes the pressure module and experimental procedures in detail and then discusses the results.

2.0 DESCRIPTION OF EXPERIMENTS

2.1 Compartmentalized Pressure Module

The pressure module, shown schematically in Figure 1a and in a photograph in Figure 1b, contains sixteen individual compartments. Using the 1:64 scale established for the building model in previous rain-wetting tests (Surry et al [1994]), these compartments measure roughly 1m by 1m in full scale dimensions (their depth was not dynamically modelled since only mean pressures were of interest). Venting was achieved through centrally located circular holes, one per compartment, covering roughly 0.5 percent of the module surface. Mean pressures were measured using three "solid state" electronic pressure scanner modules, each with sixteen channels, contained within the space below the compartments. A row of thirty-two equally-spaced external pressure taps defined the mean pressure distribution on the surface of the building and within each compartment an internal tap measured the mean cavity pressure.

The module was designed such that each individual compartment can act on its own or be connected to its neighbour. The connection was made by extending rubber tubing from the bottom side of one compartment into that of the next. Two tube connectors were provided for each interior compartment (and only one for the two outside compartments) so that any number of compartments could be joined together to act as one. The tube inlets could be sealed if not needed. This setup allowed for the following compartment arrangements:

1. 16 compartments each 1 m wide,
2. 8 compartments each 2 m wide,
3. 4 compartments each 4 m wide, and
4. 2 compartments each 8 m wide.

2.2 Building Model

The full scale dimensions of the building model are 81 m by 18 m by 60 m high according to the length scale previously established of 1:64. The model consists of a wooden plywood box enclosed by 51 mm of styrofoam. The pressure module, which also has a depth of 51 mm, could be placed at any desired location simply by cutting out a block of the styrofoam. The plywood core was slotted to accommodate the

electrical hardware extending from the pressure scanners out through the back of the module. The six locations, shown in Figure 2a, were chosen to investigate mean pressure gradients near edges, near corners and at the centre of the building. The model with the module in place is shown in Figure 2b.

The module spans roughly 20 percent of the building width when oriented horizontally and 27 percent of the building height when vertical. As designed, the module allows one-dimensional pressure gradients to be measured perpendicular to an edge starting within roughly 25 cm (full scale) of that edge. This equates to less than half a percent of either the width or height of the building. The spacing of the remaining 31 external taps, expressed once again in full scale, is approximately 50 cm. This "tight" arrangement of the external taps was chosen to ensure a high degree of resolution in the measured mean pressure gradients.

2.3 Modelling of the Wind

All experiments were conducted in the low-speed test section of the Boundary Layer Wind Tunnel II at the University of Western Ontario. This tunnel has a cross section of 5 m wide by 4 m high and a length of 52 m.

The upwind surface roughness elements used to generate the turbulent boundary layer remained the same for all tests. These elements produced a roughness length (z_o) of approximately 30 cm (full scale) which is a typical value for suburban areas. The resulting mean speed and local turbulence intensity profiles are shown in Figure 3.

In the experiments, a reference pitot-static probe was mounted approximately 2.4 m upstream and 1.1 m off-centre of the testing location at a height of about 1.8 m above the surface and was used to monitor the wind speeds. This was related to the model roof height speed by pre-established calibrations. For all tests the roof height wind speed averaged roughly 7.5 m/s in model scale.

2.4 Experimental Procedure

Under the above conditions the following experiments were performed. First, four tests were executed with the module located at position A and exposed to normal winds, each time changing only the number of compartments. The remaining tests

measured mean pressures for all module locations and a variety of wind angles, but were all performed with 8 compartments, each approximately 2 m wide and each having two vents at the 1/4 and 3/4 points. Table 1 provides a summary of the number of compartments and range of wind angles tested at each location.

Module location	No. of compartments	Wind angle, θ°
A	16, 8, 4 and 2	0
A, B and C	8	-90 to +90
D, E and F	8	0 to +90

Table 1 Summary of experiments

3.0 DISCUSSION OF RESULTS

All tests were conducted over a thirty second time period and pressures were recorded with "solid state" electronic scanners at a rate of 400 per second. These correspond in full scale to about a ten minute sample at twenty samples per second. The data were then non-dimensionalized by the local mean dynamic pressure at roof height ($0.5\rho V_H^2$) and reduced to a single mean pressure coefficient for each tap location.

Three (of approximately 12,000) instantaneous pressure traces for the normal wind case of module position A are shown in Figure 4. They illustrate the unsteady components from which the mean distribution, shown in bold, is derived. One contains the overall minimum pressure, another the overall maximum and the last contains the largest unsteady gradient, which is more than twice the local mean value. The bounding curves shown in this figure also demonstrate the large range of pressures experienced at any given location for a fixed mean wind direction over a period of about ten minutes in full scale. In reality, of course, the turbulence in the wind changes the local wind speed and direction, leading to the observed fluctuations.

Figure 5 shows the same mean pressure distribution together with the corresponding cavity pressures plotted as discrete points. Note that the compartments are paired together to act as eight individuals, whose lateral extent is indicated by the vertical dashed lines. Each of these compartments contained two internal taps. This plot displays slight differences in mean cavity pressures within

a joined compartment. Some of these differences reflect experimental variability, but they also suggest that, as air travels in one vent hole and out the other, minor losses occur within the tubing and result in small pressure differences. These losses have been estimated in Appendix 1 and are compared to the head loss occurring through the vent holes.

The bulk of the experimental results are presented graphically in Appendix 2 (Figures A2.1 to A2.40) with a common format. Each figure shows the distribution of external mean pressures (Cpe) acting on the surface of the building and the net mean pressures (Cpe - Cpi) applied to the rainscreen. The vertical dashed lines shown in the lower plot of net pressures illustrate the number of compartments considered and their lateral extent. The pressure within each compartment (Cpi) has been calculated* and shown between the vertical dashed lines. Illustrations depicting the module location and wind angle are provided in each figure.

It is very important to note that the internal pressures in these compartments are dependent on the number and location of the vents, as well as on the external pressure distribution across the compartment. For example, in Figure 5 (and Figure A2.5) where there are two vents per compartment at the 1/4 and 3/4 points, the compartment pressures roughly average the external pressures over the compartment. However, if only a single vent had been used, the internal pressure would have simply reflected the external pressure at that point. In the extreme case of a single vent placed at the edge of the compartment, the residual pressure difference in Figure A2.5 could then be essentially doubled and be of either sign, depending on which edge of the compartment was vented.

It is also important to note that the fact that an entire compartment is within a negative pressure region (for example, the edge compartment in Figure 5), does not eliminate the potential for the residual pressures to drive water, if present, into the cavity. For any such cavity in a gradient with more than one venting point, the cavity pressure will always be between the pressures acting at the vents, causing air to flow in at one location and out at another. For the edge compartment of Figure 5, the flow would be into the cavity through the vent furthest from the edge. If the

---

* Mean cavity pressures were calculated by averaging all internal taps within a compartment.

vent holes were placed at the edges of the compartment, then larger flows (and a different cavity pressure) would result. Only if the vents merged to a single vent, would there be no flow into the cavity (although there would still be net pressures across the wall away from the single opening).

Figures A2.1a to A2.1d verify that smaller compartments reduce the net pressures acting on the rainscreen. With compartments 1 m wide and central venting (Figure A2.1a) the largest net pressure and suction coefficients are roughly 0.14 and -0.24 and increase to about 0.17 and -0.65 when the compartment width is 8 m with 8 uniformly-spaced vents (Figure A2.1d). These pressure coefficients were obtained by extrapolating to the extreme edges of the rainscreen - i.e. from the extreme edge of the building to the centre of the first compartment divider.

The remaining figures in Appendix 2 show results of all module locations and wind angles tested with 2 m wide compartments. The following observations have been made:

1. For perpendicular wind, large horizontal mean pressure gradients occur near the side edges of windward walls and large vertical gradients occur near the top edges (Figures A2.5 and A2.36).
2. Large vertical mean pressure gradients also occur on the upstream building corner with 45 degree winds (Figure A2.23).
3. It is the large gradients which cause the lack of pressure equalization of rainscreens. When the external mean pressure distribution is nearly constant, the net pressures on the rainscreen essentially reduce to zero (Figures A2.26 to A2.35).

Of all tests performed, the second condition described above produced the largest external mean pressure gradient occurring over the width of one compartment. Cpe changed by roughly 1.2 over the width of the edge compartment (i.e. 2 m). This equates to roughly 260 Pa/m in full scale using the method described below.

All mean pressure coefficients (Cp) presented in this report may be converted to actual full scale mean pressures (P) using the equations shown below:

mean external pressure on building: $Pe = q_H \cdot Cpe$
mean internal compartment pressure: $Pi = q_H \cdot Cpi$
mean net rainscreen pressure: $Pnet = q_H \cdot (Cpe-Cpi)$

In the above equations q_H represents the mean dynamic pressure at the 60 m height of the building. Using a typical 10 year dynamic pressure of 300 Pa at 10 m, q_H (where H = 60 m) equates to about 430 Pa using the NBCC simple approach*. This value has been used to estimate a nominal mean pressure that may occur across the rainscreen of 2 m edge compartments with vents at the 1/4 and 3/4 points (see Table 2). The direction of wind which caused the largest edge gradient at each module location has also been included. Note, once again, that the net pressures were obtained by extrapolating to the extreme limits of the edge compartment, and that their absolute values are determined by where the cavity is vented (i.e. the resulting cavity pressure). However their total range (positive minus negative) is independent of cavity venting. Note also that the pressures acting to drive water through the vents will be less than the values listed here for vents at the 1/4 and 3/4 marks, and will also be dependent on vent locations.

Module location	Range of net pressures	Wind angle, θ°, causing largest mean gradient
A	70 Pa to -170 Pa	0 and +30
B	90 Pa to -60 Pa	+45
C	90 Pa to -430 Pa	+45
F	80 Pa to -200 Pa	0, ±30 and ±45

Table 2 Approximate range of net mean pressures across the rainscreen for 2 m wide edge compartments with vents at the 1/4 and 3/4 width locations

* This approach is used for cladding pressures and is representative of open country conditions and, therefore, overestimates the mean pressures for suburban areas.

Figures 6a and 6b compare the horizontal mean pressure distribution at mid-height (i.e. module positions A and E) for a perpendicular wind with similar results obtained by Lin and Inculet [1994]. Their distributions were obtained from a geometrically-similar building model (comparable aspect ratios of each model are provided in the figures) exposed to a slightly different wind profile. The Cp's obtained by Lin and Inculet were multiplied by a correction factor to account for the difference in the mean dynamic pressures at the mid-height level of the respective building models. The shape of the mean pressure distributions compare remarkably well but results from this study display somewhat lower pressures. Although this alteration in magnitude has little effect on the gradients, which are the main focus of this work, the differences were investigated further.

The authors believe that part of this discrepancy results from blockage in the wind tunnel for model orientations with θ near 0°. For other wind angles, there is less blockage. The wind tunnel blockage (ratio of model frontal area to wind tunnel working section area) in this study is approximately 6% for $\theta = 0°$, compared to less than 0.5% in Lin's experiments. The latter value is essentially unconstrained freestream flow which parallels full scale conditions. With 6% blockage the wake is prevented from expanding as it would under unconstrained conditions which results in lower leeward or wake pressures (i.e. higher negative pressures). Reduced wake pressures translate into a reduction in pressure at the edge of the windward face of the building. Blockage is not expected to affect the maximum positive pressure near the centre of the building. Thus, the differences seen there, in Figure 6a, must be due to other factors, such as the different turbulent wind simulations which may alter the mean flow aerodynamics somewhat. Near the edge, as seen in Figure 6b, the differences are larger and these additional differences are attributed to blockage.

A quantitative study of blockage corrections by McKeon and Melbourne [1971] showed that the mean change in wake pressure on surface-mounted rectangular plates exposed to turbulent boundary layer flow can be found by;

$$\Delta Cp_b = -2.7 \cdot C_{Dt} \cdot (S/C)$$

where S/C is the ratio of frontal model area to wind tunnel area (i.e. blockage). ΔCp_b represents the average decrease in mean pressure on the leeward face as compared to freestream or "unblocked" flows. C_{Dt} (the total drag coefficient of the model) varies with both aspect ratio (model height to width) and blockage ratio. In this study the

aspect and blockage ratios are 0.74 and 0.06 respectively for $\theta = 0°$. Hence, using data from McKeon and Melbourne, the drop in base pressure is predicted to be approximately 0.15, which is consistent with the increased discrepancy displayed in Figure 6b at the edge, as compared to the central area in Figure 6a.

Parkinson and Jandali [1970] used a theoretical method to determine the mean pressure distribution on a two-dimensional flat plate for perpendicular uniform flow. The horizontal mean pressure distribution at mid-height from this study has also been compared with their results (see Figure 6c). The dissimilar approaching wind characteristics have again been approximately accounted for by normalizing to the mean dynamic pressure of the approaching wind at the mid-height of the building. The distribution derived by Parkinson and Jandali displays somewhat steeper gradients as the edge is approached; however, the agreement is remarkable considering that in the theoretical model, air flows around the plate in only two dimensions and hence has a much more negative leeward pressure than the experimental model. The discrepancy in the central positive pressure region is also explainable in that the theoretical model in two dimensions attains a $Cp = +1.0$ whereas the three dimensional model attains only a $Cp \approx +0.6$, due to the flows in the third dimension.

Both sets of comparisons are encouraging. Any residual errors in the mean pressure gradients are probably within the range of variability for actual full scale applications, when varying terrain and neighbouring buildings are considered.

A SUMMARY OF THIS WORK IS PRESENTED AT THE BEGINNING.

REFERENCES

Baskaran, A. [1992], "Review of Design Guidelines for Pressure-Equalized Rainscreen Walls", Internal Report No. 629, National Research Council, Institute for Research in Construction, Ottawa, Canada.

Lin, J-X and D. R. Inculet [1994], "A Study of Statistically Representative Mean Pressure Gradients", An interim progress report to CMHC, The Boundary Layer Wind Tunnel Laboratory, The University of Western Ontario, March 21, 1994.

Mckeon, R.J. and W. H. Melbourne [1971], "Wind Tunnel Blockage Effects and Drag on Bluff Bodies in a Rough Wall Boundary Layer", Proceedings of the 3rd International Conference of Wind Effects on Building and Structures, Tokyo, 1971, pp. 263-272.

Parkinson, G. E. and T. Jandali [1970], "A Wake Source Model for Bluff Body Potential Flow", Journal of Fluid Mechanics, 1970, vol. 40, part 3, pp. 577-594.

Surry, D., D. R. Inculet, P. F. Skerlj, J-X. Lin and A. G. Davenport [1994], "Wind, Rain and the Building Envelope: A Status Report of Ongoing Research at the University of Western Ontario", Proceedings of the Invitational Seminar on Wind, Rain, and the Building Envelope, The University of Western Ontario, London, May 16 - 18, 1994.

Vickery, B. J. and Karakatsanis, C. [1989], "Discharge Coefficients And Internal Pressures in Well Ventilated Buildings", Proceedings of the 2nd Asia-Pacific Conference on Wind Engineering, Bejing, China, June, 1989, Vol. 1, pp. 557-567.

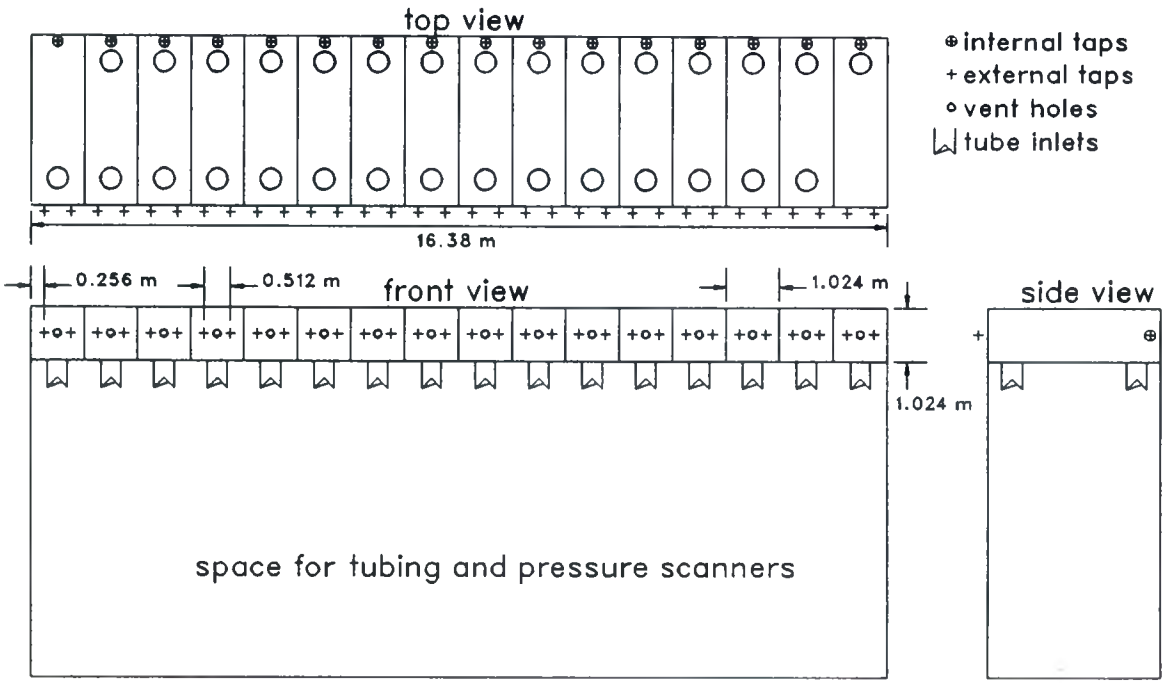

Figure 1a Schematic of pressure module

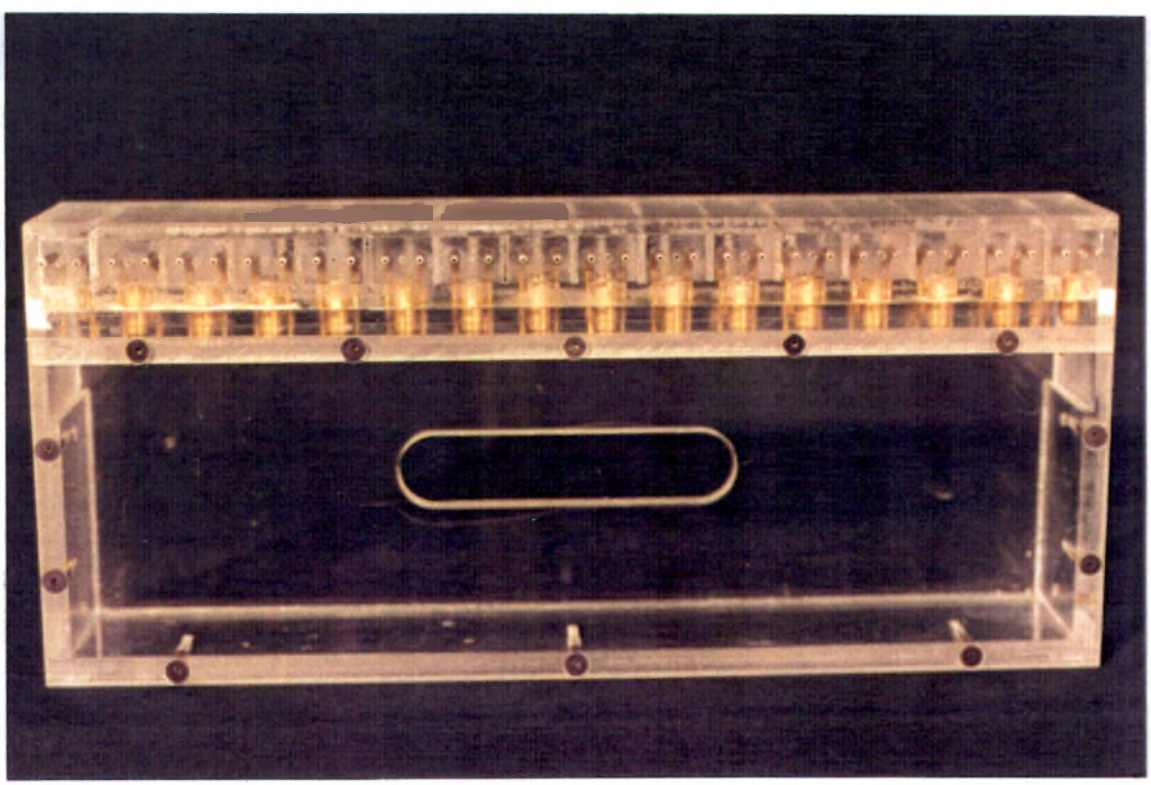

Figure 1b Photograph of pressure module

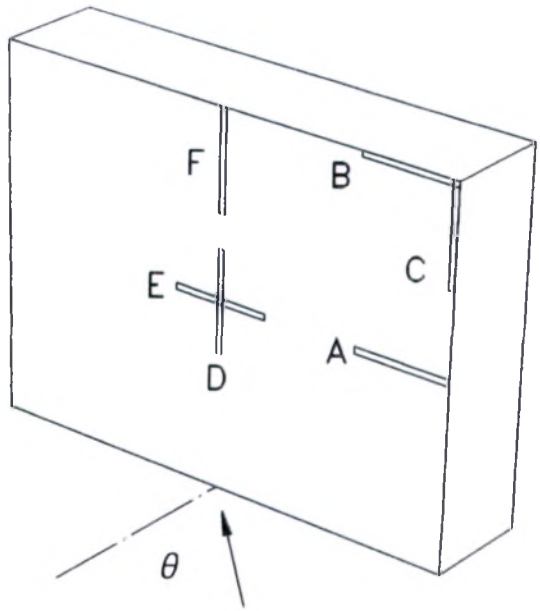

Figure 2a Module locations and defining wind angle

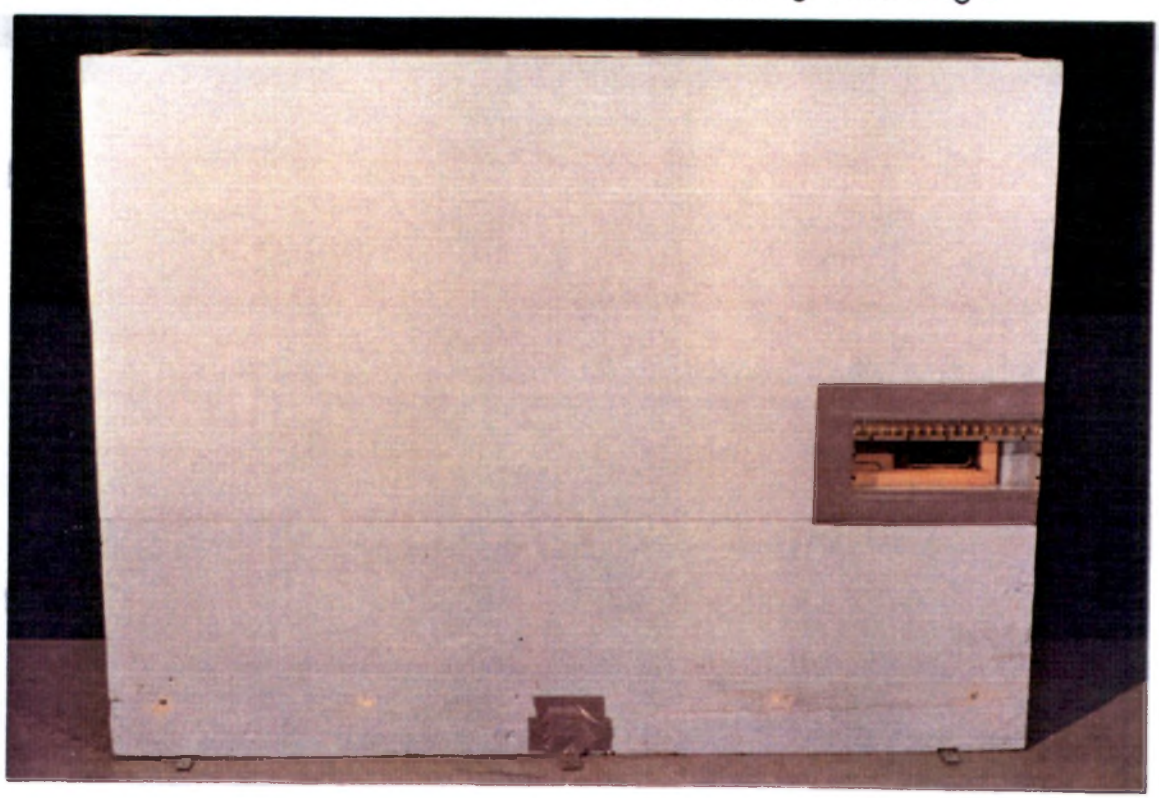

Figure 2b Photograph of building model with module in location A

RPR601 VERTICAL PROFILE EXPOSURE=6 DATE 17/09/93

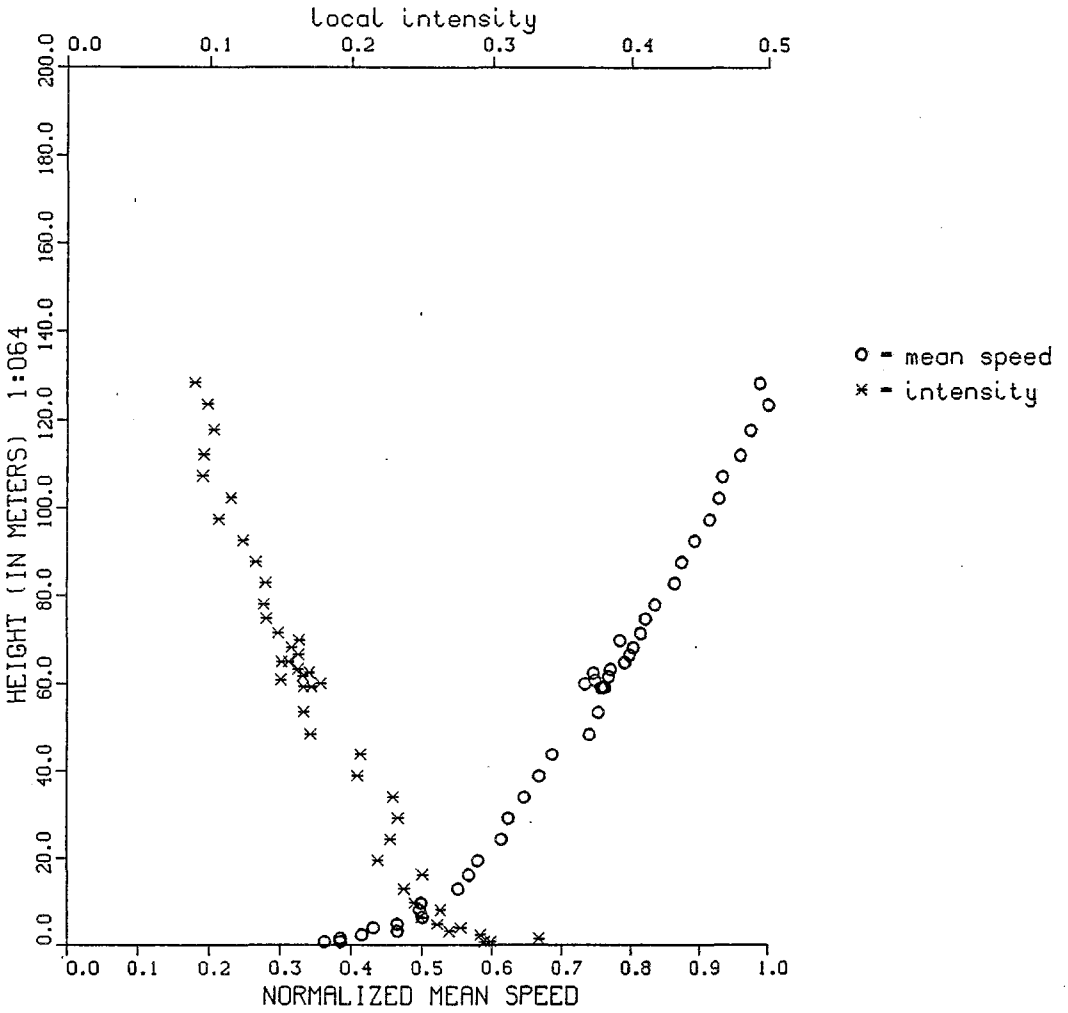

Figure 3 Mean speed and turbulence intensity profiles at test site

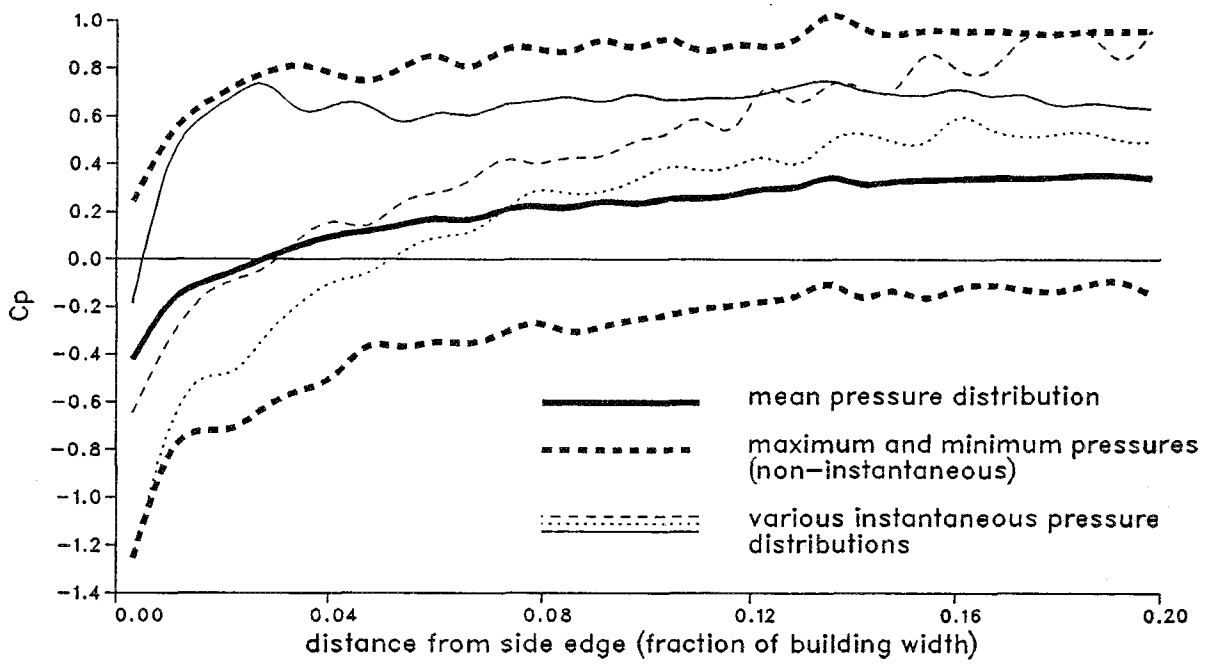

Figure 4 Pressure distributions on the external building surface near an edge (module location = A and $\theta = 0^{\circ}$)

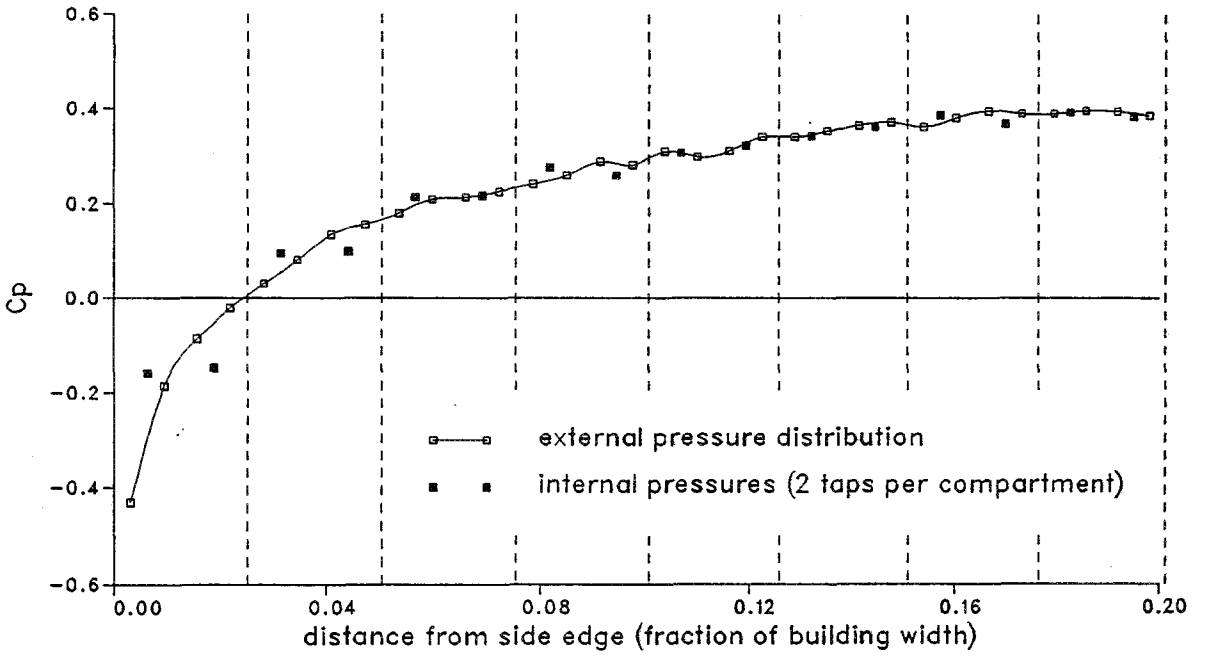

Figure 5 Mean pressure distribution and mean cavity pessures within 8 compartments (module location = A and $\theta = 0^{\circ}$)

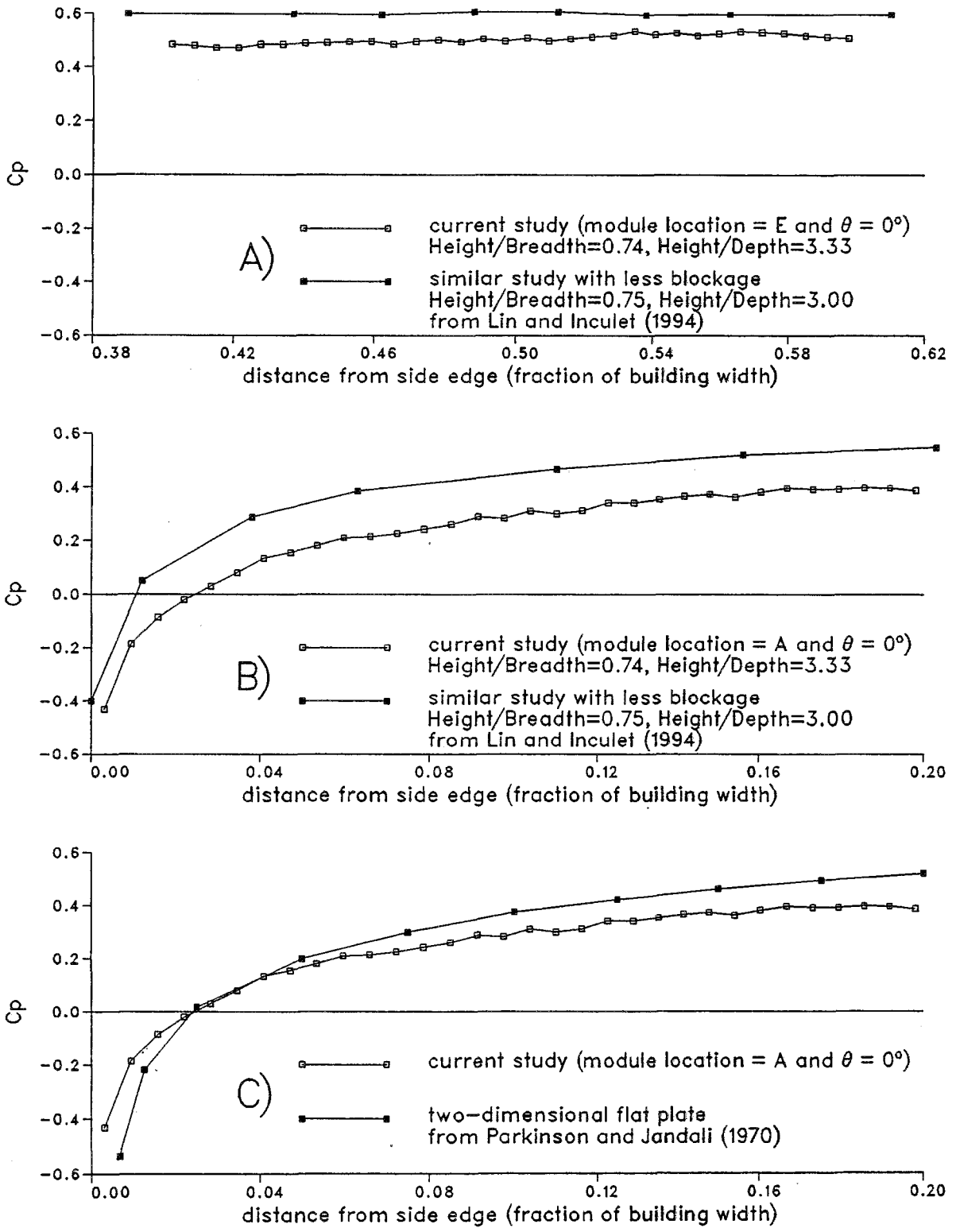

Figure 6 Comparisons of external mean pressure distributions

APPENDIX 1

COMPARISON OF LOSSES THROUGH VENTS TO LOSSES THROUGH TUBING

The pressure module was designed such that individual compartments could be joined together with rubber tubing and hence the total number of compartments could be altered. Two compartments are effectively joined if the losses through the tubing are negligible compared to the losses through the vent holes. These relative losses are estimated below.

Figure A1.1 schematically shows two individual compartments joined to act as one (which was the configuration for 40 of 43 experiments) and also defines various parameters. The compartment is exposed to an external pressure gradient such that air enters through the vent of cavity A and exits through the vent of cavity B.

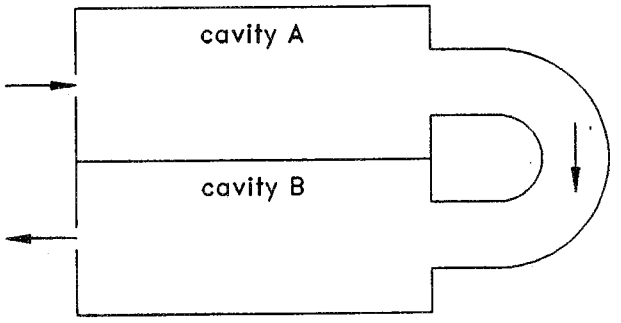

D_v = diameter of vents ≈ 1.3 mm
D_t = diameter of tubing ≈ 4.5 mm
L_t = length of tubing ≈ 85 mm
V_v = air velocity through vents
V_t = air velocity through tubing
P_{ai} and P_{bi} = cavity pressures
P_{ae} and P_{be} = external pressures at vents
υ = viscosity of air ≈ $1.45*10^{-5}$ m^2/s
ρ = density of air

Figure A1.1 Defining sketch

The head loss through the connecting tube can be found from;

$$H_{Lt} = [K_{entrance} + K_{exit} + 2 \cdot K_{90°elbow} + fL_t/D_t]\ V_t^2/2g \qquad (1)$$

where:

$$K_{entrance} \approx 0.5,\ K_{exit} \approx 1.0,\ K_{90°elbow} \approx 0.9$$

Assuming that the tube flow is laminar*, the friction factor can be obtained by:

$$f = 64/Re = 64\upsilon/V_tD_t \qquad (2)$$

Combining equations 1 and 2 yields:

$$H_{Lt} \approx [3.3 + 3.9/V_t]\ V_t^2/2g \qquad (3)$$

* For laminar flow: $Re = V_tD_t/\upsilon < 2000$ or $V_t < 6.4$ m/s (confirmed later)

The head loss through a vent hole can be divided into losses upstream and downstream of the vena contracta. The upstream value is negligible compared to the downstream value. Therefore, the loss through a vent can be approximated by a reservoir type exit from the vena contracta area. Hence for two vents;

$$H_{Lv} \approx [2 \cdot K_{exit}] \, V_o^2/2g \qquad (4)$$

where V_o is the velocity within the vena contracta. The contraction coefficient C_c for a reservoir entrance is approximately 0.59. From continuity:

$$C_c A_v V_o = A_t V_t$$

$$\Rightarrow \quad V_o = A_t V_t / C_c A_v \qquad (5)$$

Substituting equation 5 into equation 4 yields;

$$H_{Lv} \approx 825 \, V_t^2/2g \qquad (6)$$

and from equations 3 and 6 the ratio of vent to tube losses becomes:

$$H_{Lv}/H_{Lt} \approx 825/[3.3 + 3.9/V_t] \qquad (7)$$

Since the difference in cavity pressures ($P_{ai} - P_{bi}$) is known from experiment and must equal the head loss through the connecting tube, V_t can be estimated from equation 3. This yields:

$$P_{ai} - P_{bi} = [3.3 + 3.9/V_t] \, \rho V_t^2/2 \qquad (8)$$

By expressing P_{ai} and P_{bi} as pressure coefficients and solving for V_t, equation 8 becomes;

$$V_t \approx [-3.9 + (15.2 + 13.2 \, V_h^2 \cdot \Delta Cpi)^{0.5}]/6.6 \qquad (9)$$

where V_h is the established tunnel speed at model height and is equal to 7.5 m/s. Using equations 9 and 7 together with experimental values of ΔCpi, the ratio H_{Lv}/H_{Lt} is found to be typically 35. It should also be noted that V_t remained well below the laminar threshold and was typically around 0.2 m/s.

Uncertainties arise in the above analysis associated with the determination of loss factors, particularly where flows are venting into a high speed attached airflow (see Vickery and Karakatsanis [1989]).

As a further check, the external pressure distribution can be used to determine an expected ΔCpi, based on the loss equations above. Equating the difference of the external mean pressures at the vents to the total loss through the compartmentalized unit leads to the following expression for V_t:

$$V_t \approx [-3.9 + (15.2 + 3310 \, V_h^2 \cdot \Delta Cpe)^{0.5}]/1655 \qquad (10)$$

The largest ΔCpe from experiments is 0.52 which, through elimination of V_t from equations 9 and 10, results in a ΔCpi of 0.015. The measured ΔCpi during the same

experiment is 0.017 and compares well with the expected value determined above, hence supporting the assumptions.

It appears that the module design essentially provided for tubing losses that were much smaller than vent losses, and hence it behaves satisfactorily for larger compartments.

APPENDIX 2

EXPERIMENTAL RESULTS

list of figures

Figures	Module location	Wind angle, θ	Compartment width
A2.1a to A2.1d	A	0°	1, 2, 4 and 8 m
A2.2 to A2.9	A	-90° to +90°	2 m
A2.10 to A2.17	B	-90° to +90°	2 m
A2.18 to A2.25	C	-90° to +90°	2 m
A2.26 to A2.30	E	0° to +90°	2 m
A2.31 to A2.35	D	0° to +90°	2 m
A2.36 to A2.40	F	0° to +90°	2 m

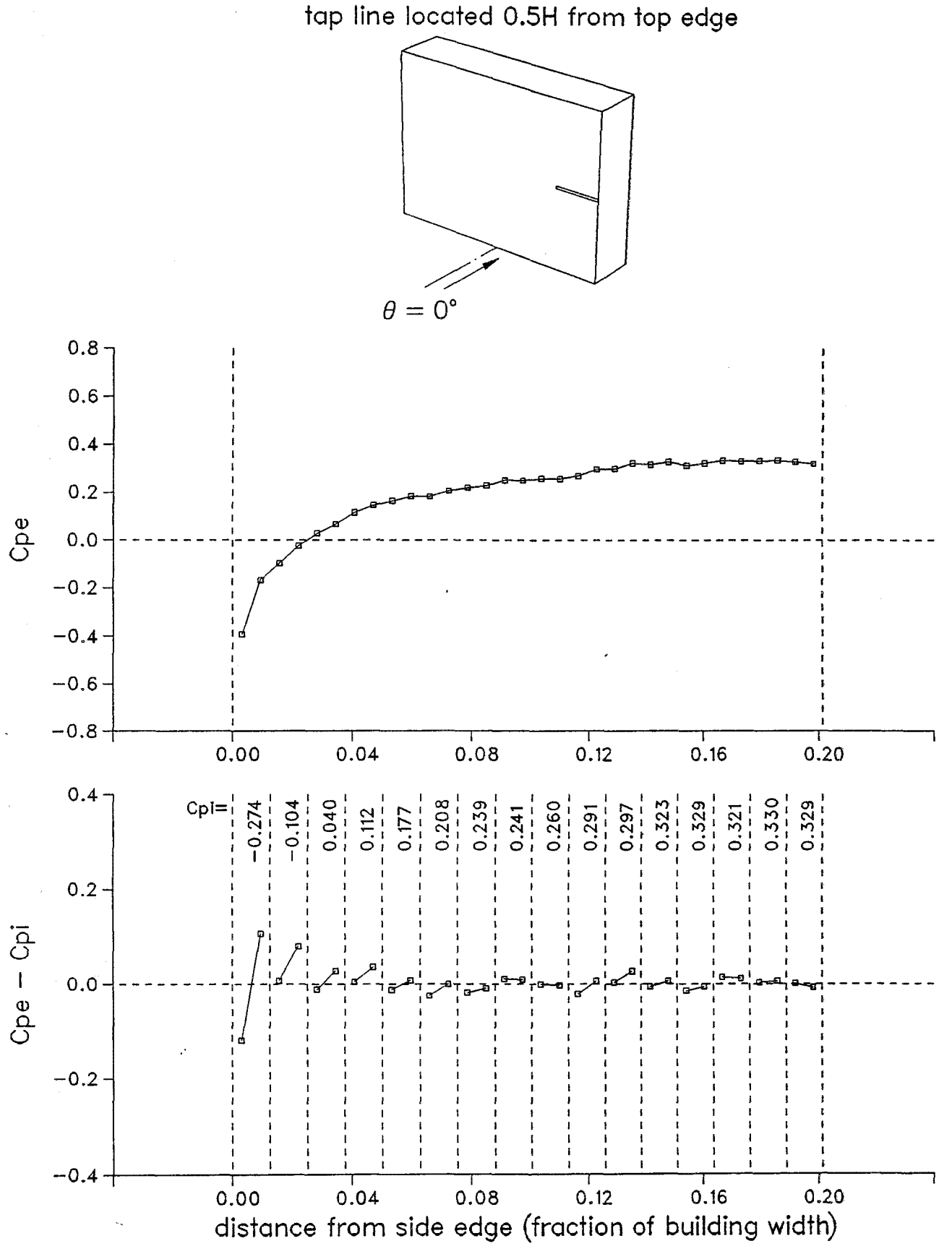

Figure A2.1a Mean pressure distribution on the building surface and the net pressure distribution across the rainscreen with 16 compartments

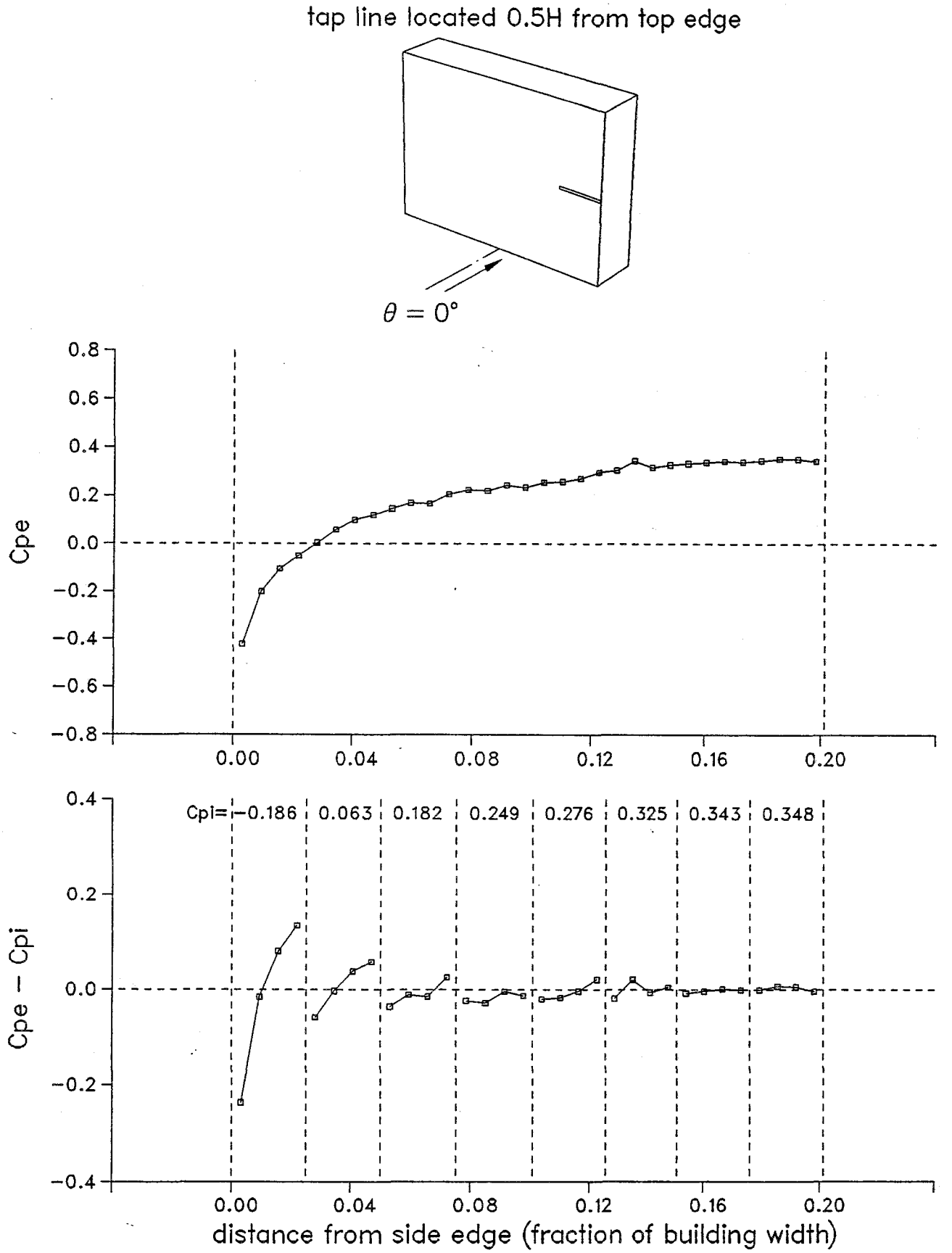

Figure A2.1b Mean pressure distribution on the building surface and the net pressure distribution across the rainscreen with 8 compartments

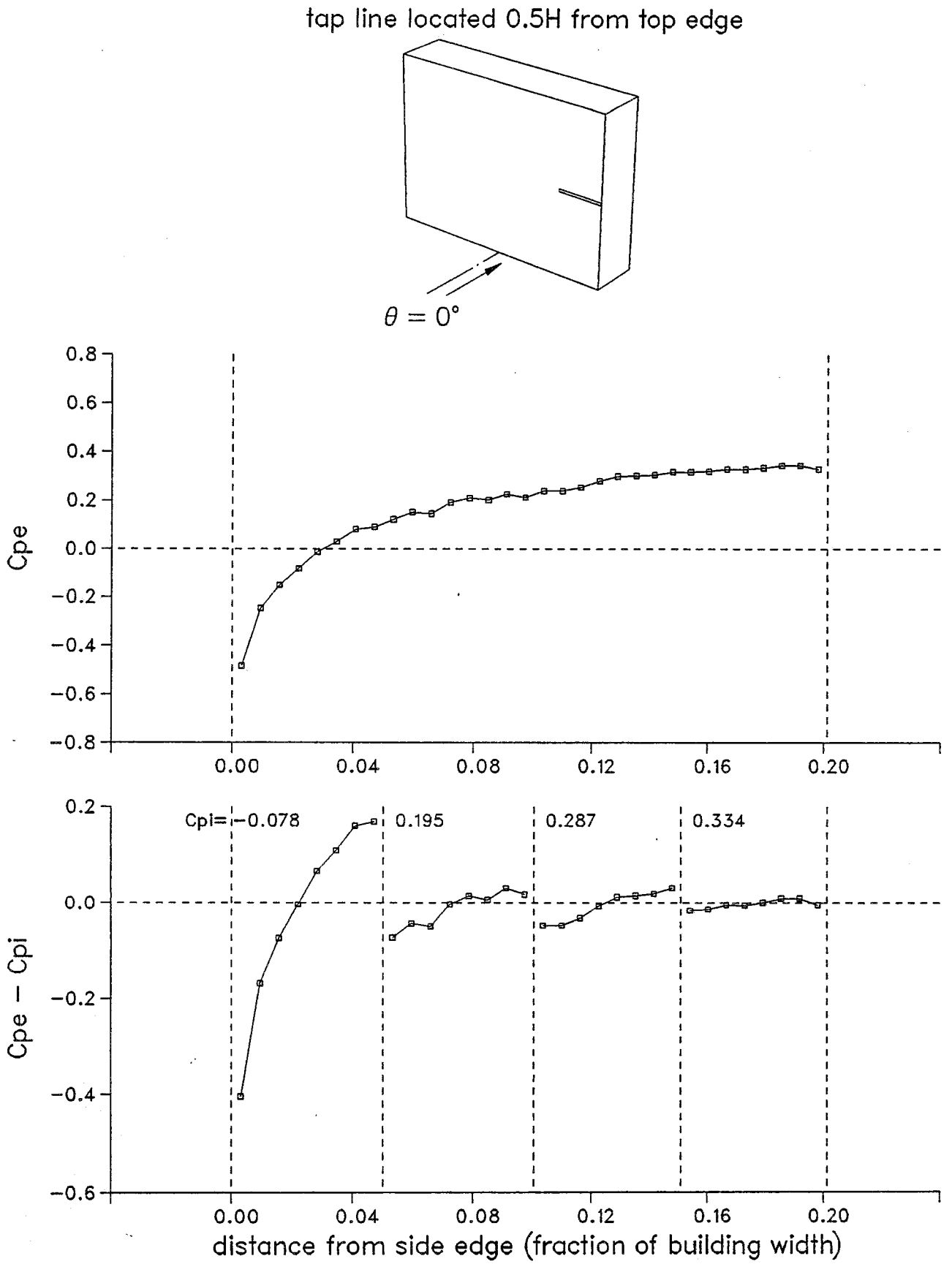

Figure A2.1c Mean pressure distribution on the building surface and the net pressure distribution across the rainscreen with 4 compartments

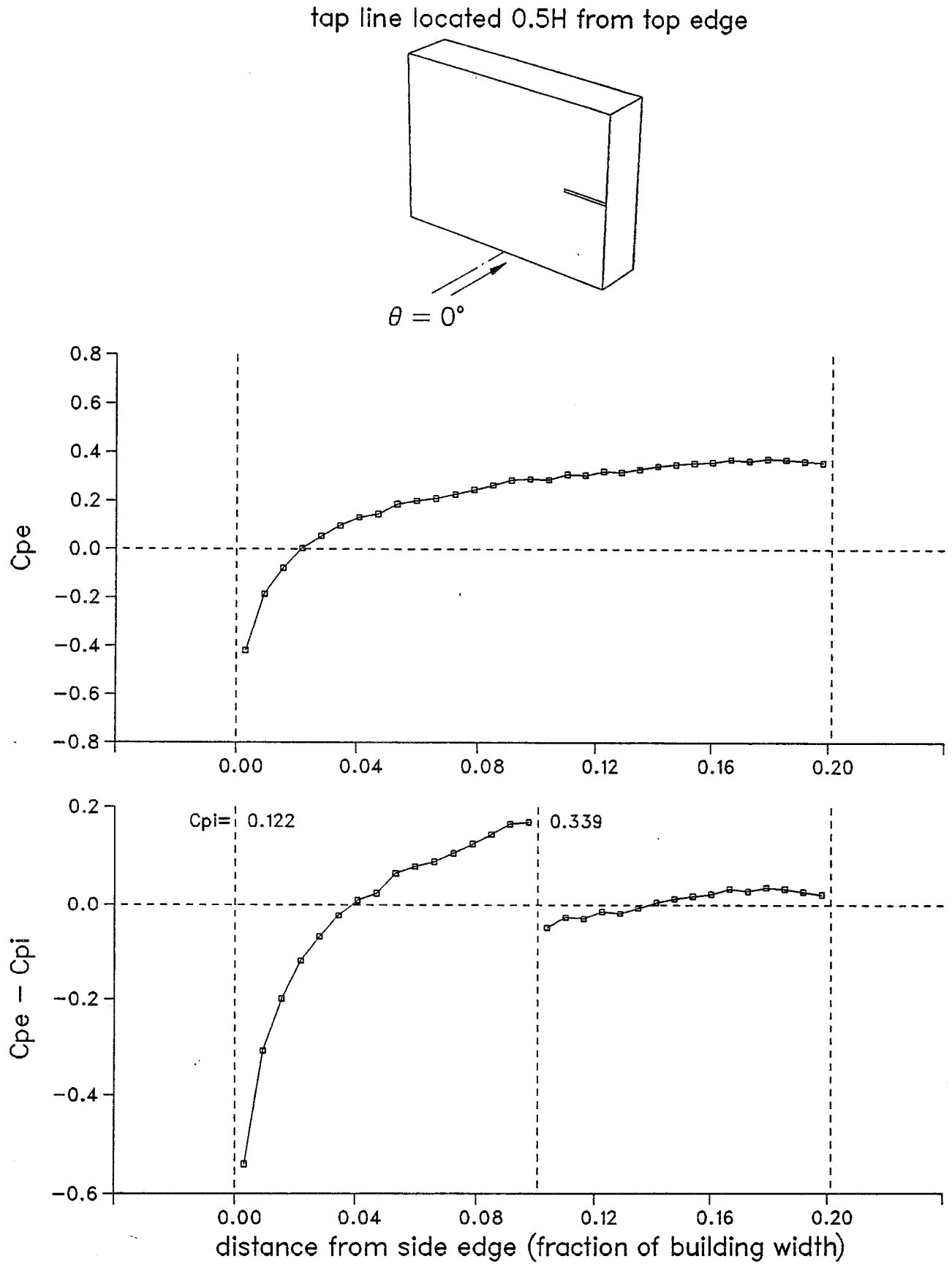

Figure A2.1d Mean pressure distribution on the building surface and the net pressure distribution across the rainscreen with 2 compartments

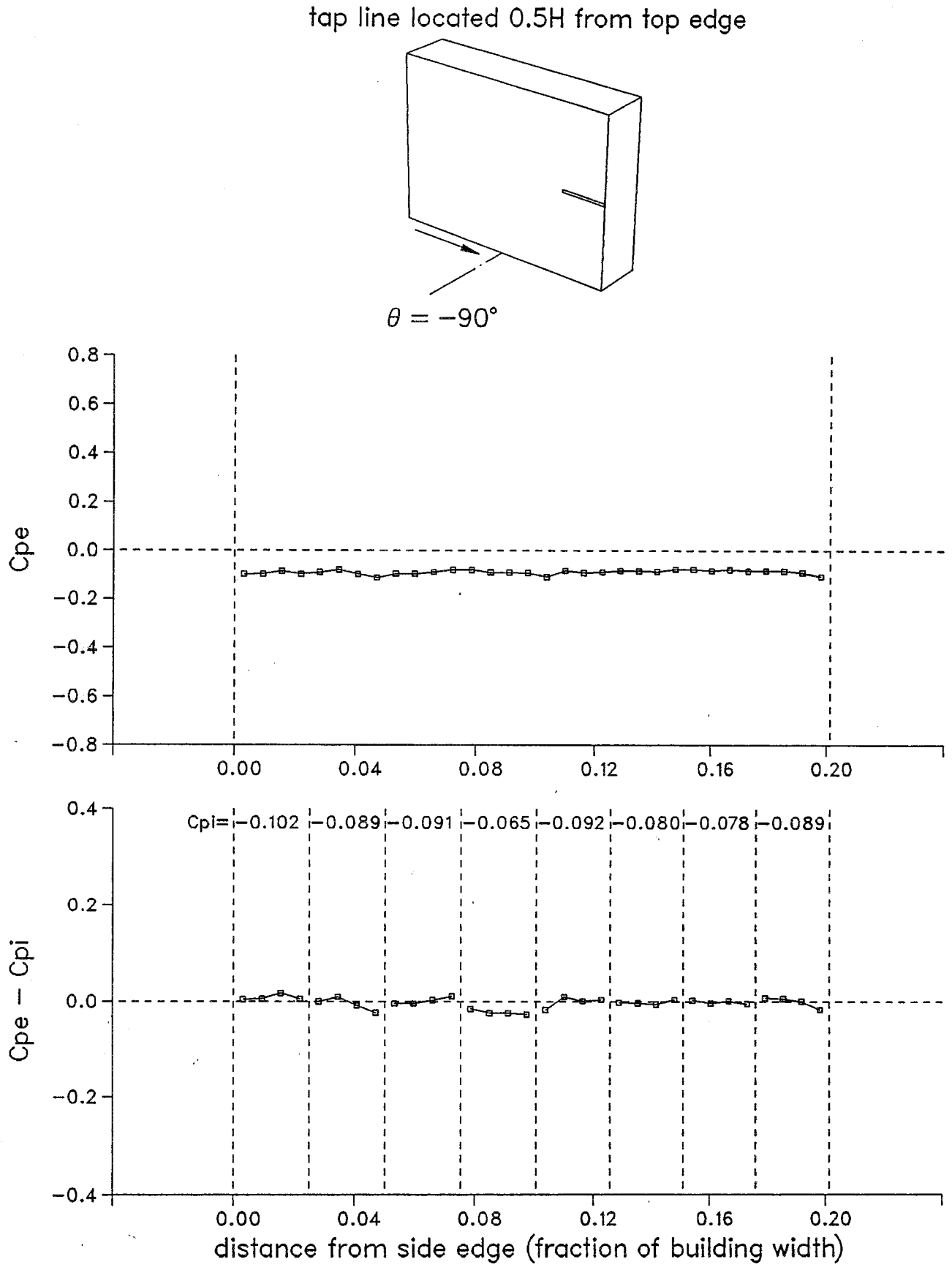

Figure A2.2 Mean pressure distribution on the building surface and the net pressure distribution across the rainscreen with 8 compartments

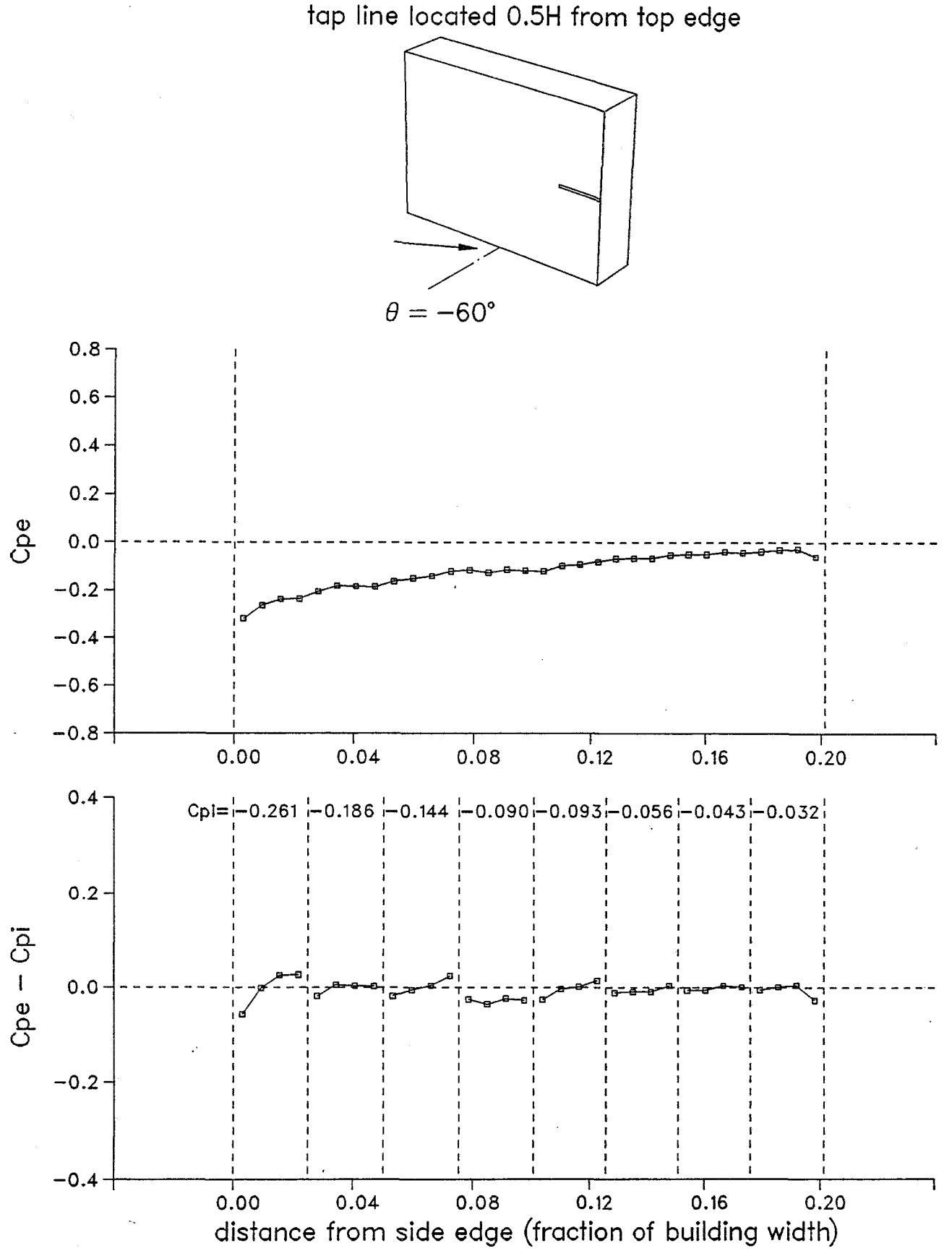

Figure A2.3 Mean pressure distribution on the building surface and the net pressure distribution across the rainscreen with 8 compartments

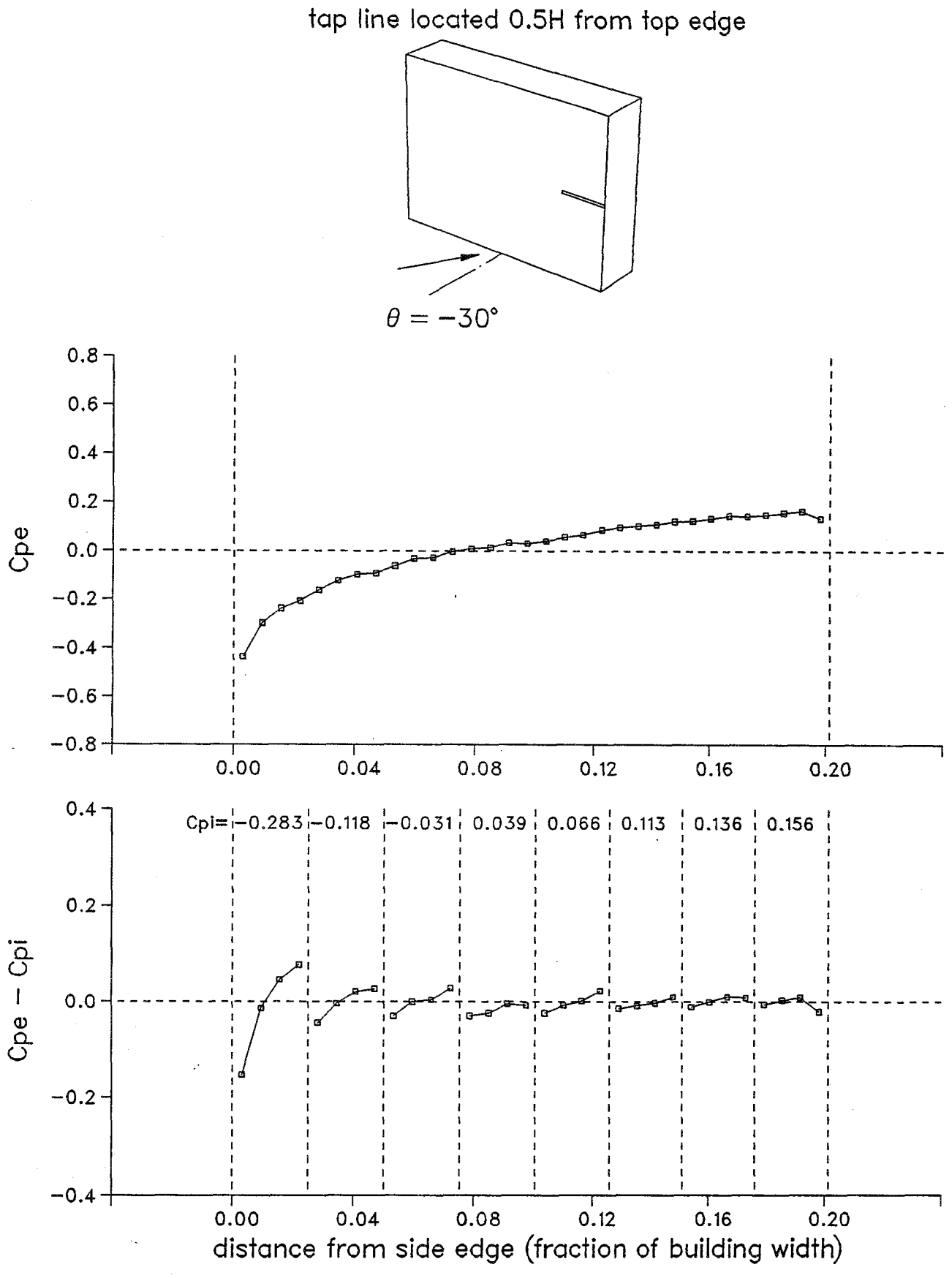

Figure A2.4 Mean pressure distribution on the building surface and the net pressure distribution across the rainscreen with 8 compartments

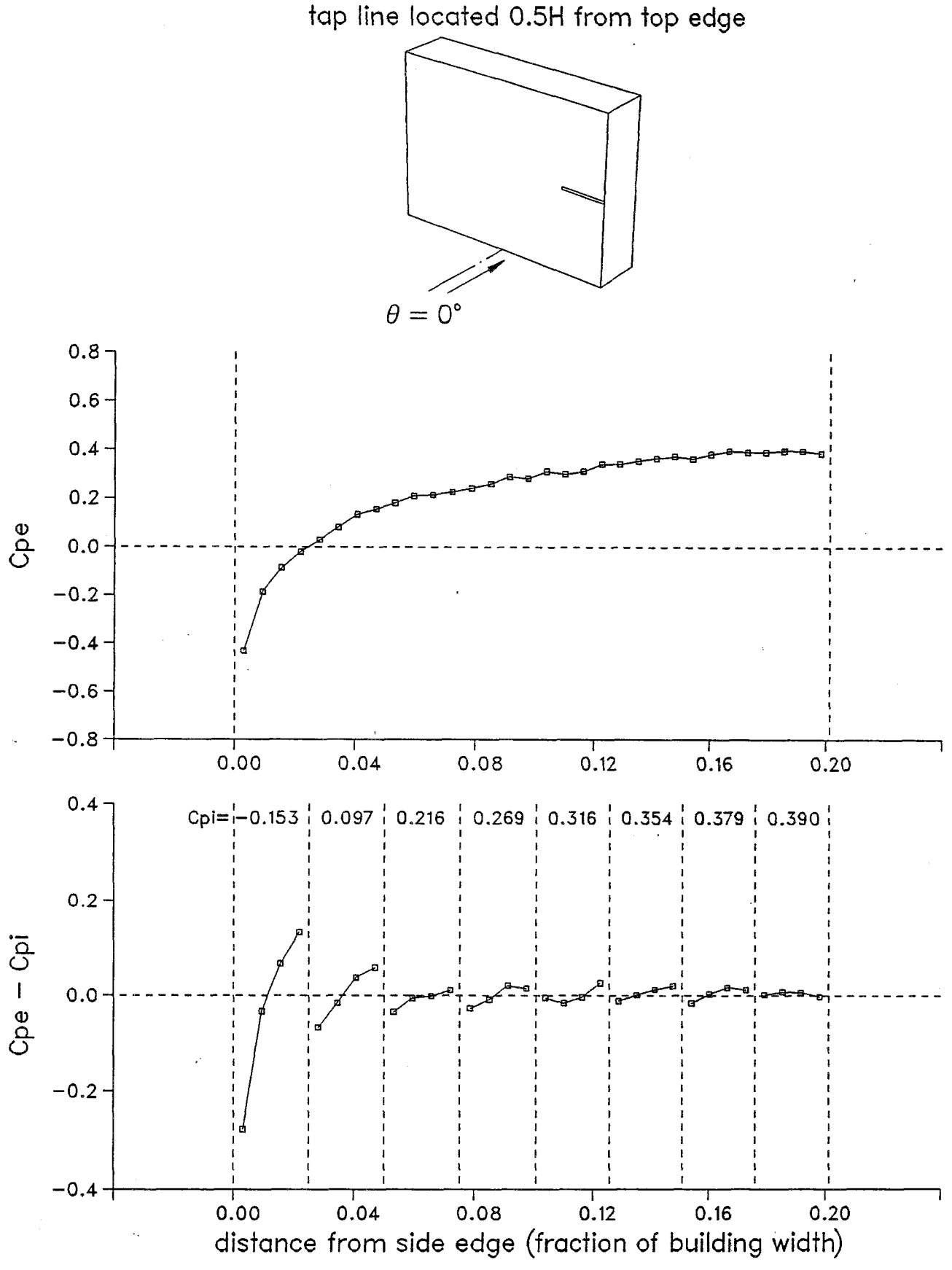

Figure A2.5 Mean pressure distribution on the building surface and the net pressure distribution across the rainscreen with 8 compartments

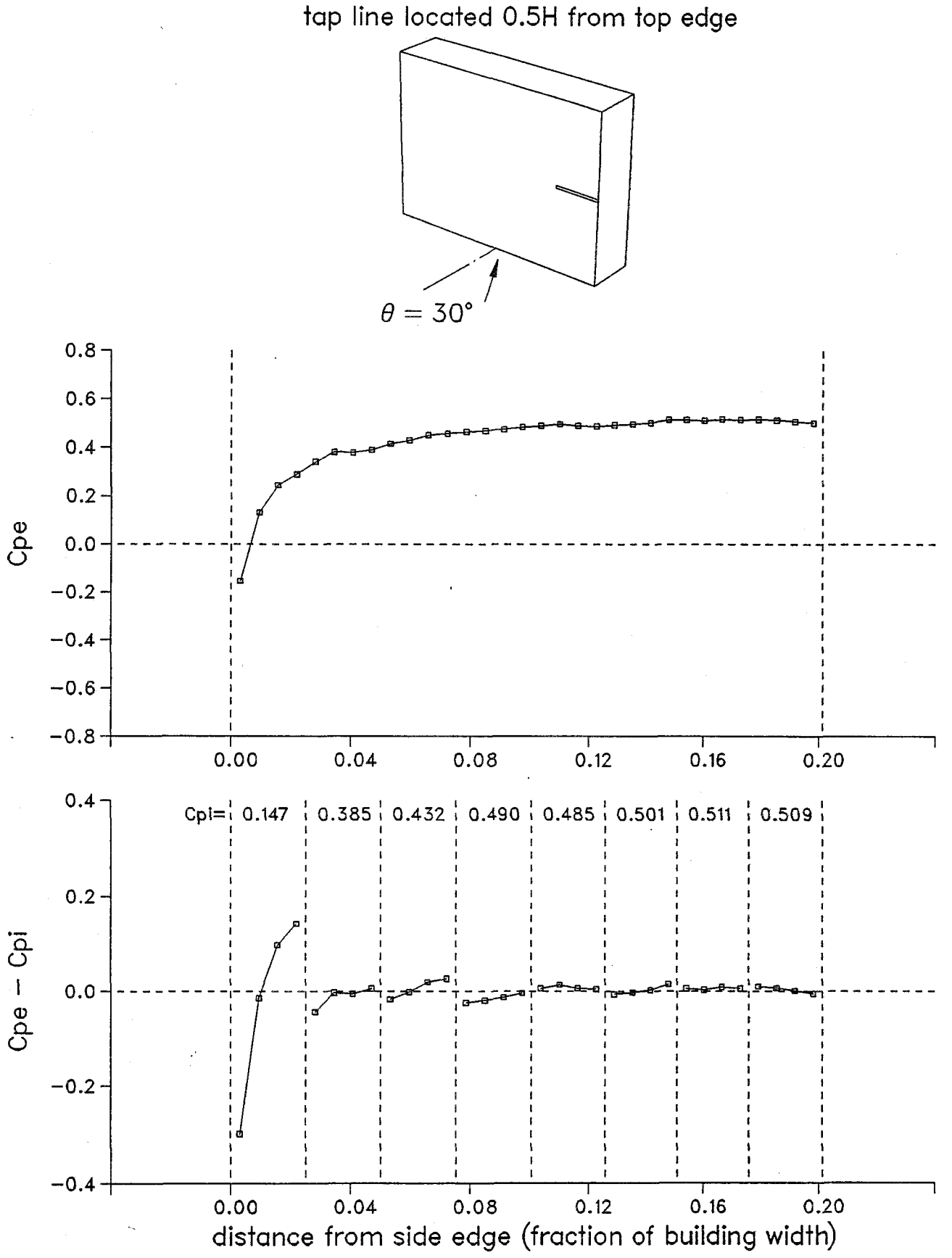

Figure A2.6 Mean pressure distribution on the building surface and the net pressure distribution across the rainscreen with 8 compartments

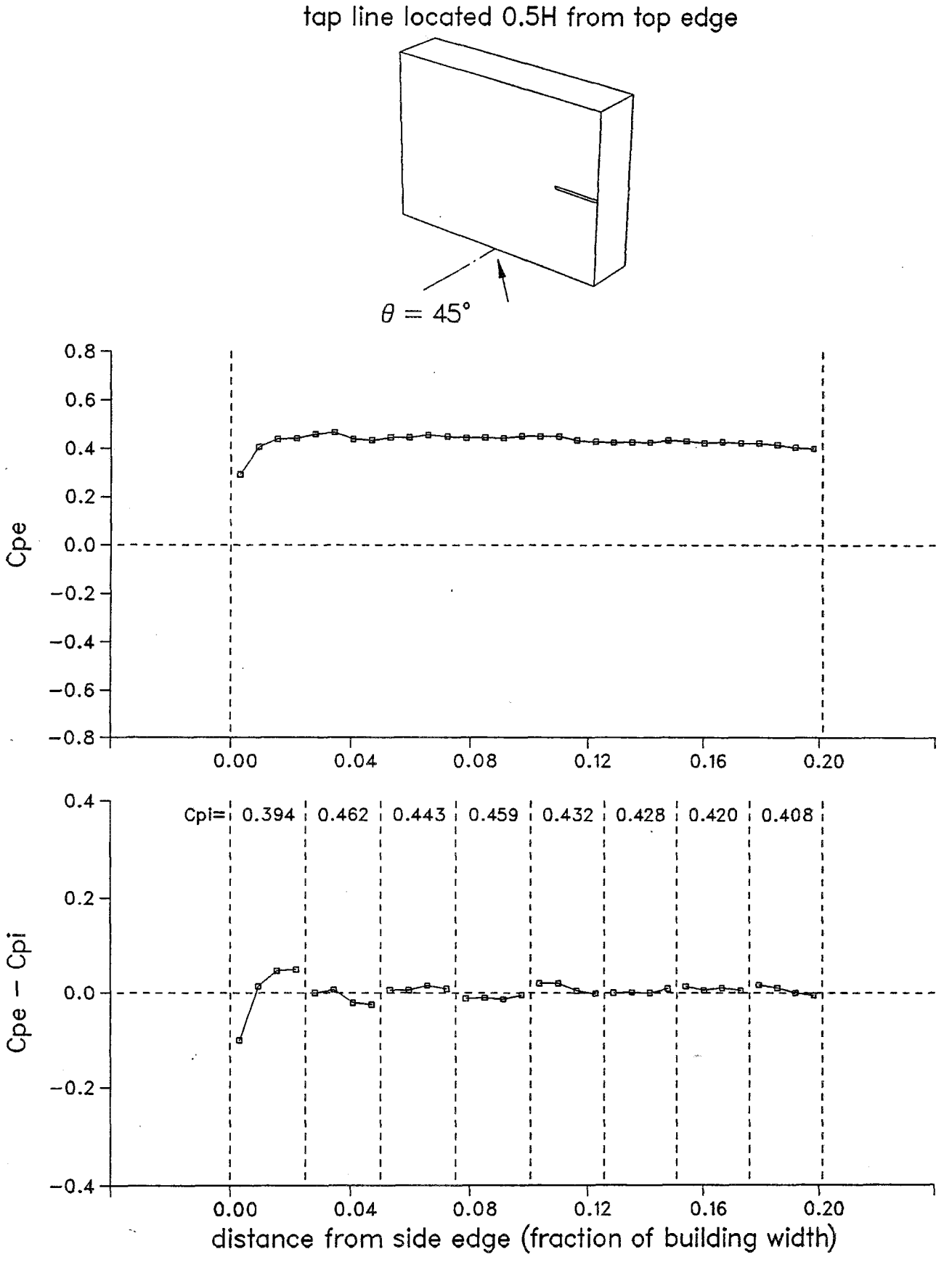

Figure A2.7 Mean pressure distribution on the building surface and the net pressure distribution across the rainscreen with 8 compartments

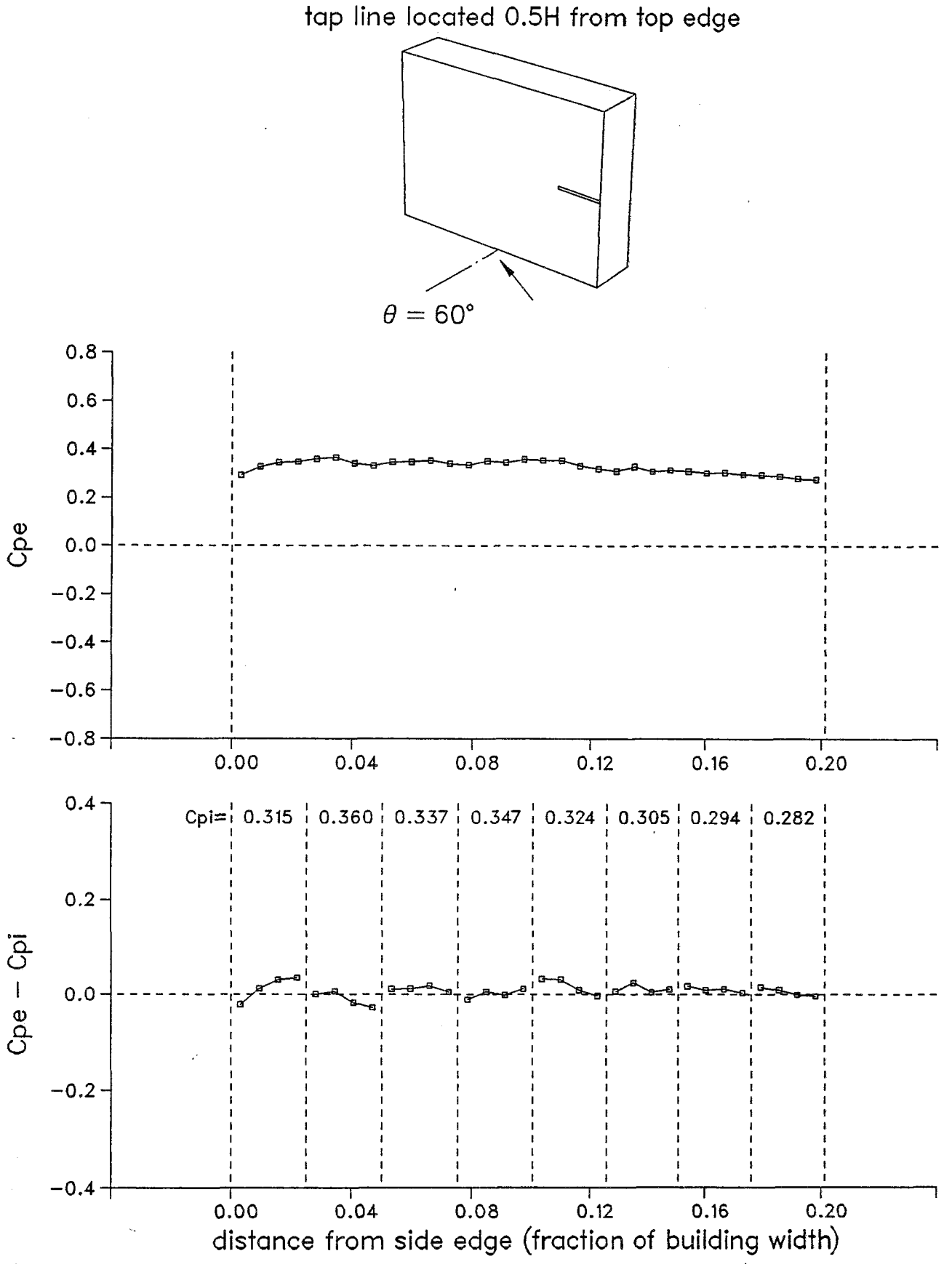

Figure A2.8 Mean pressure distribution on the building surface and the net pressure distribution across the rainscreen with 8 compartments

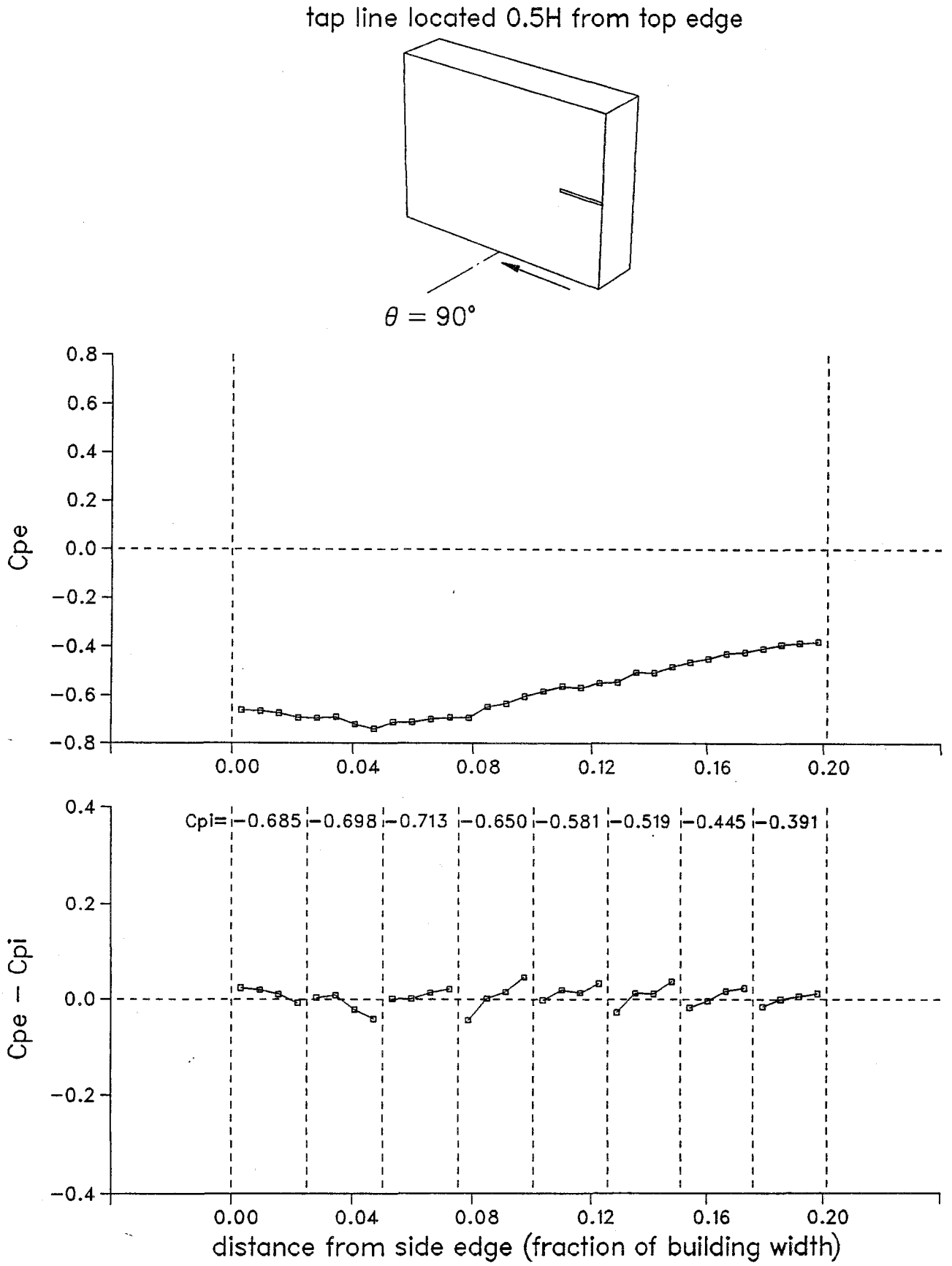

Figure A2.9 Mean pressure distribution on the building surface and the net pressure distribution across the rainscreen with 8 compartments

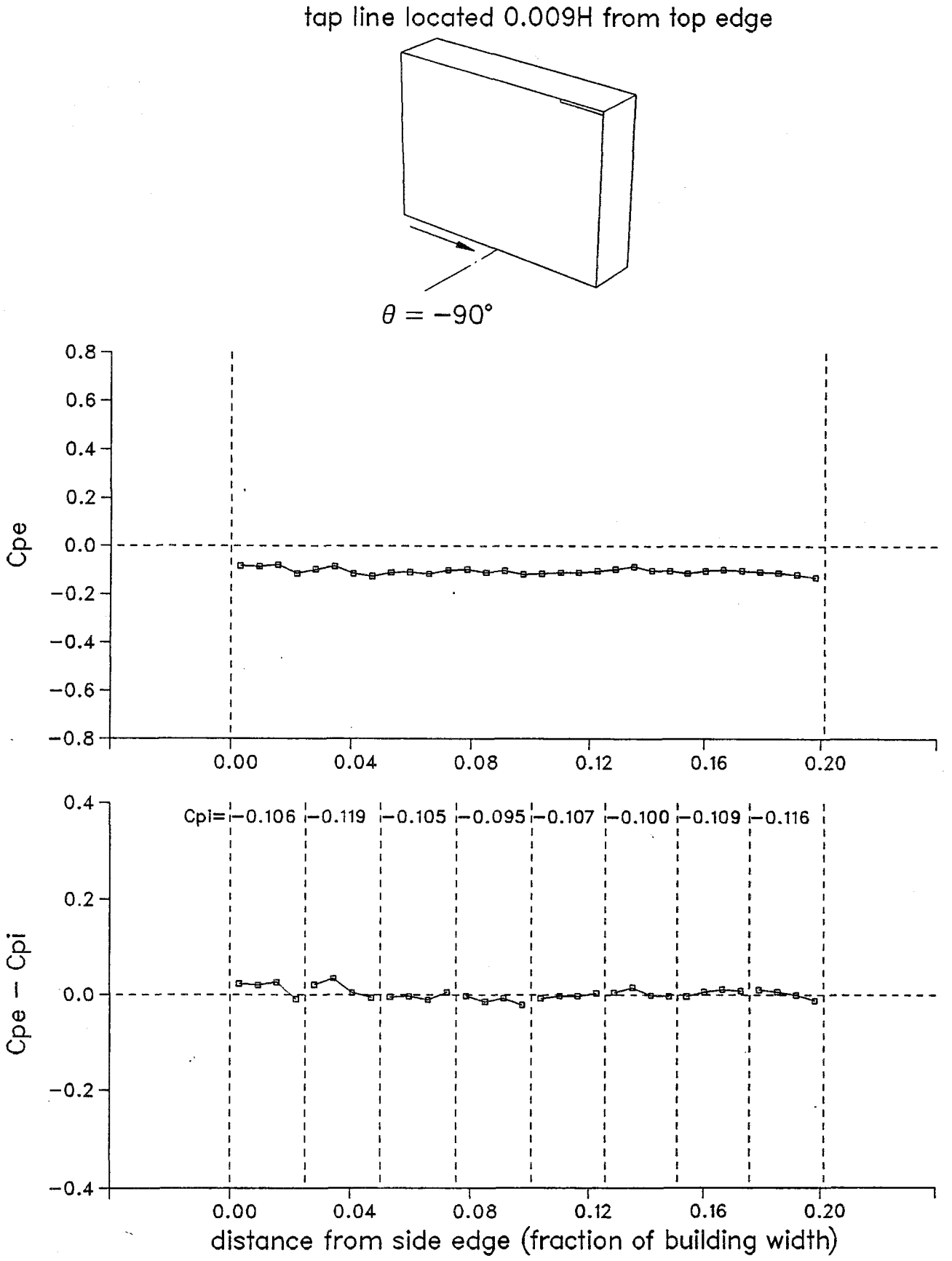

Figure A2.10 Mean pressure distribution on the building surface and the net pressure distribution across the rainscreen with 8 compartments

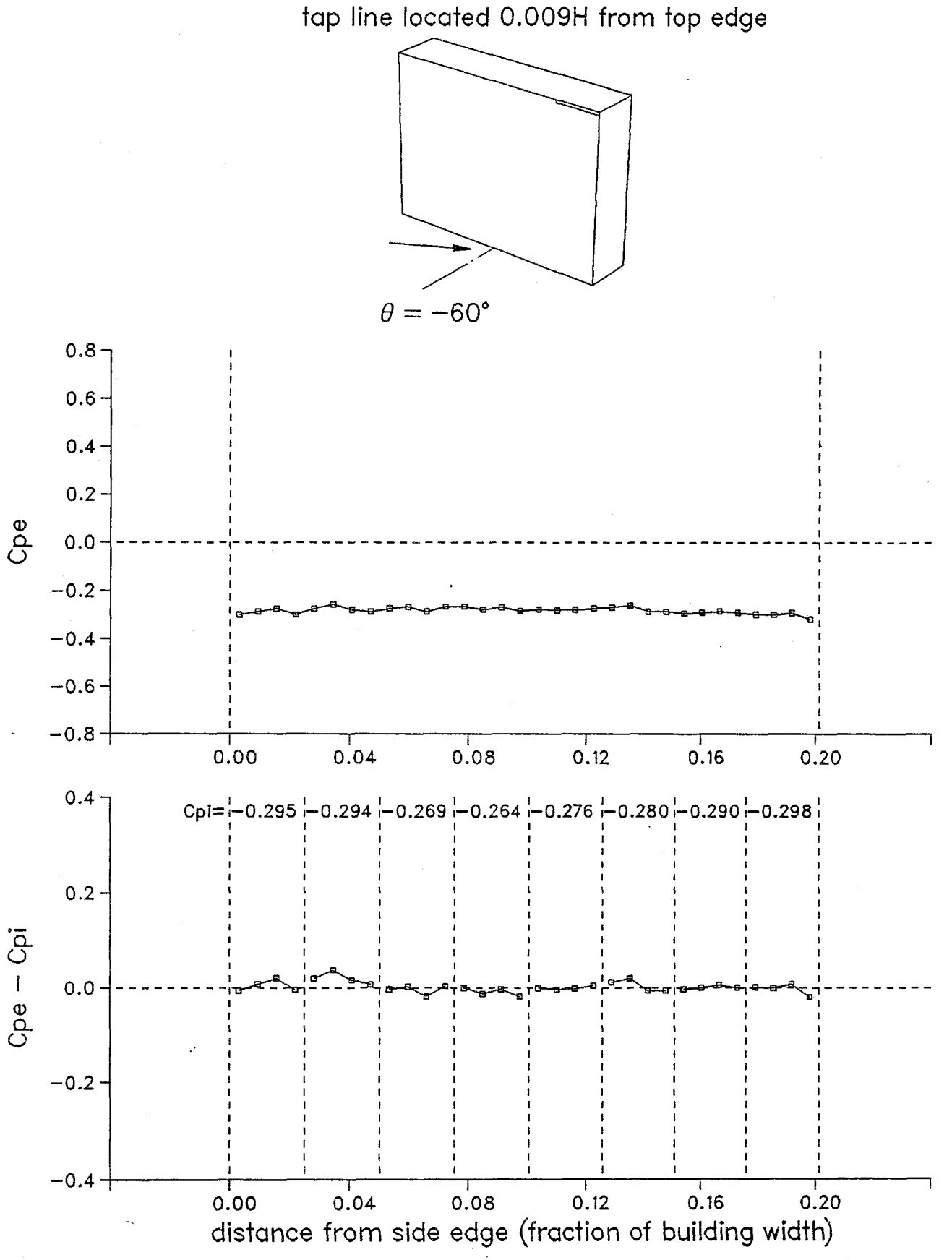

Figure A2.11 Mean pressure distribution on the building surface and the net pressure distribution across the rainscreen with 8 compartments

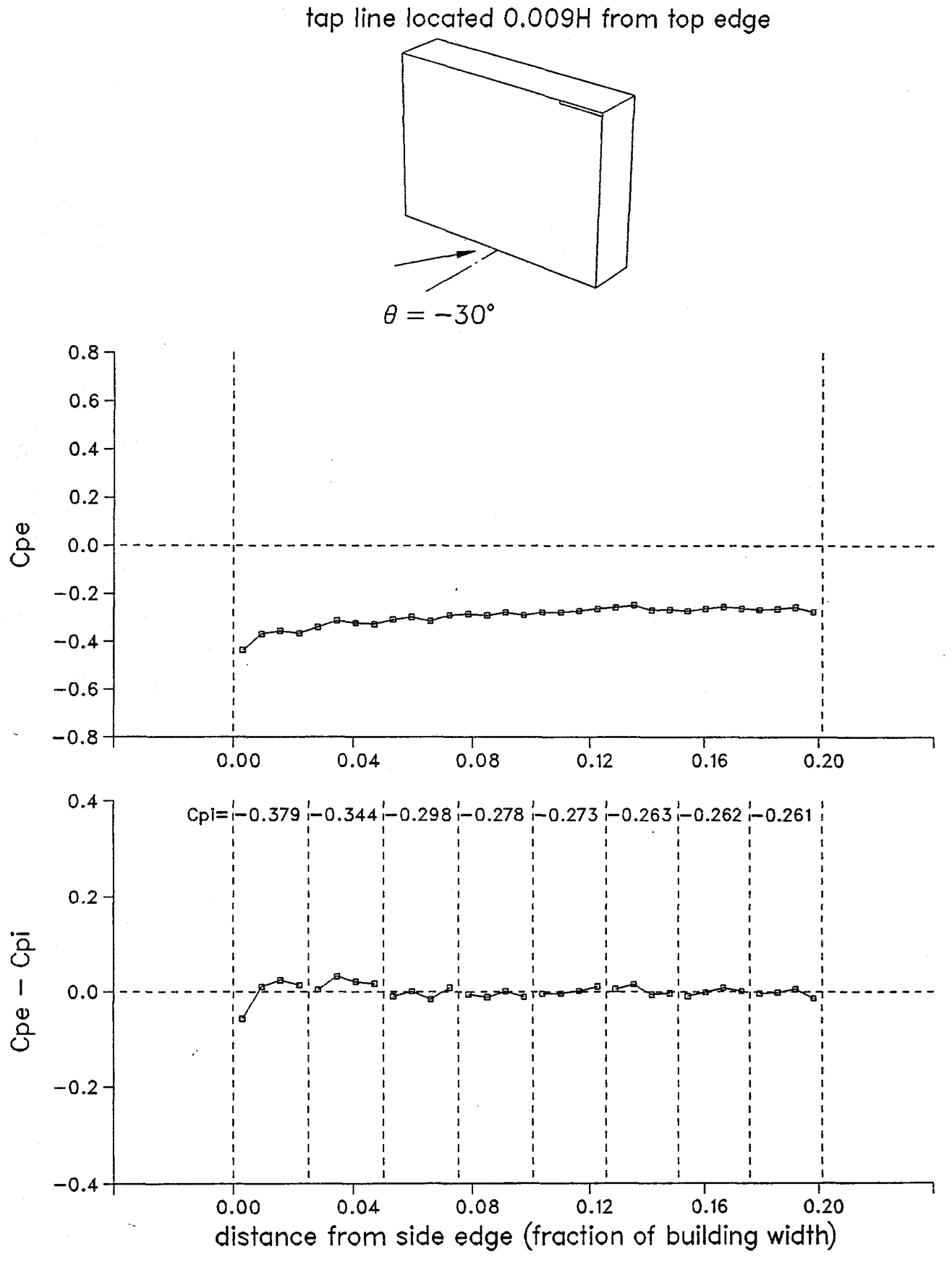

Figure A2.12 Mean pressure distribution on the building surface and the net pressure distribution across the rainscreen with 8 compartments

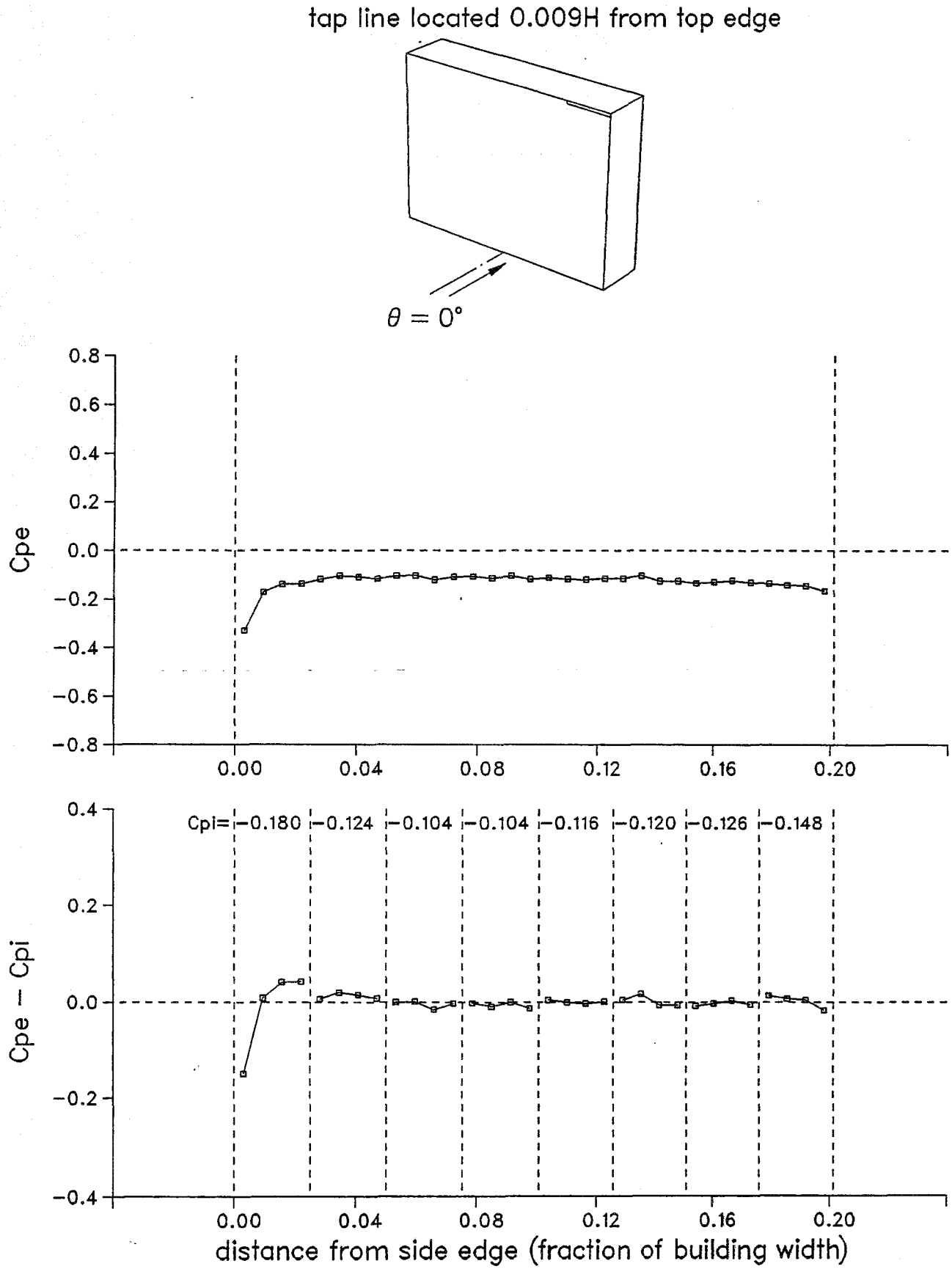

Figure A2.13 Mean pressure distribution on the building surface and the net pressure distribution across the rainscreen with 8 compartments

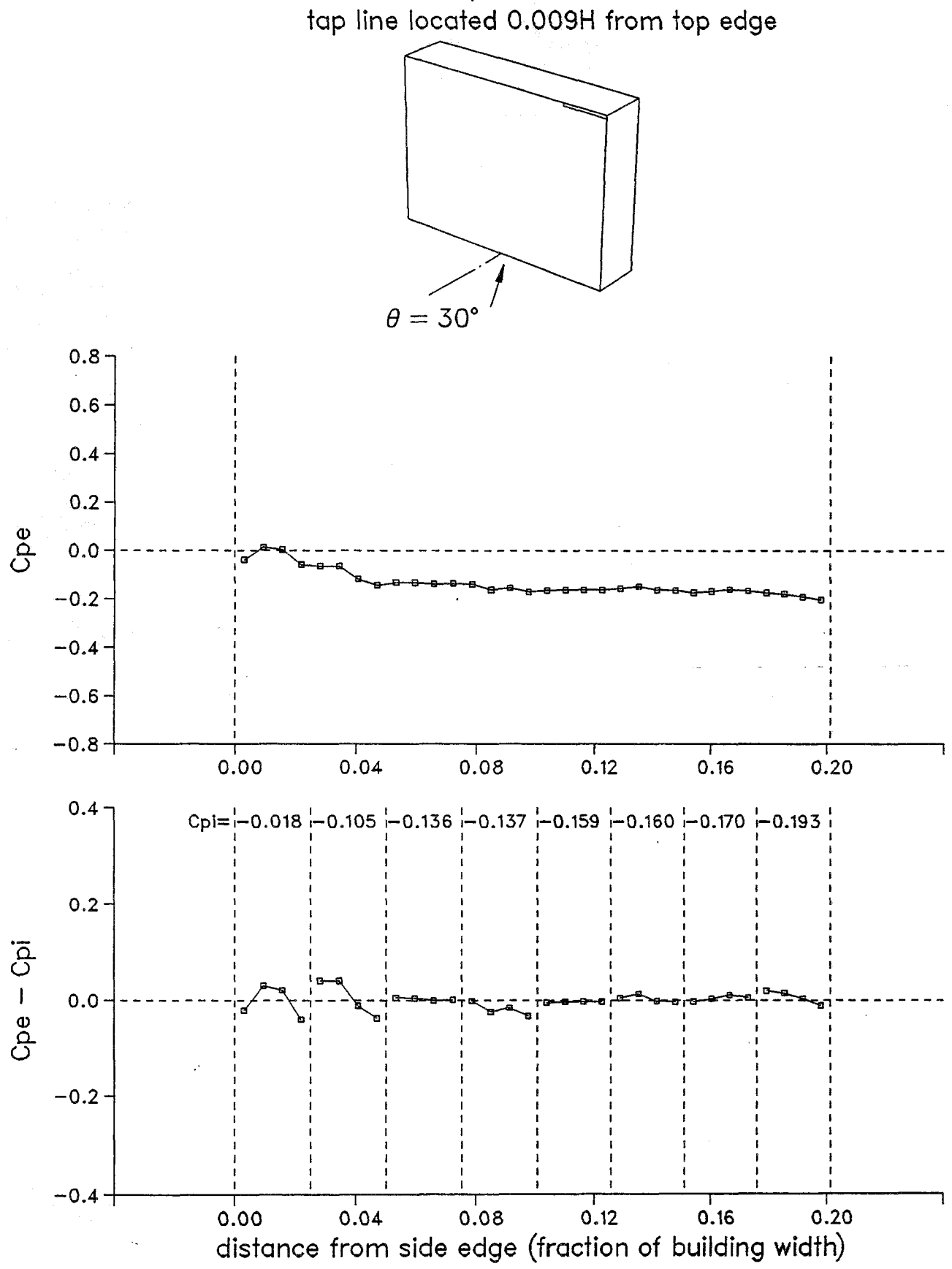

Figure A2.14 Mean pressure distribution on the building surface and the net pressure distribution across the rainscreen with 8 compartments

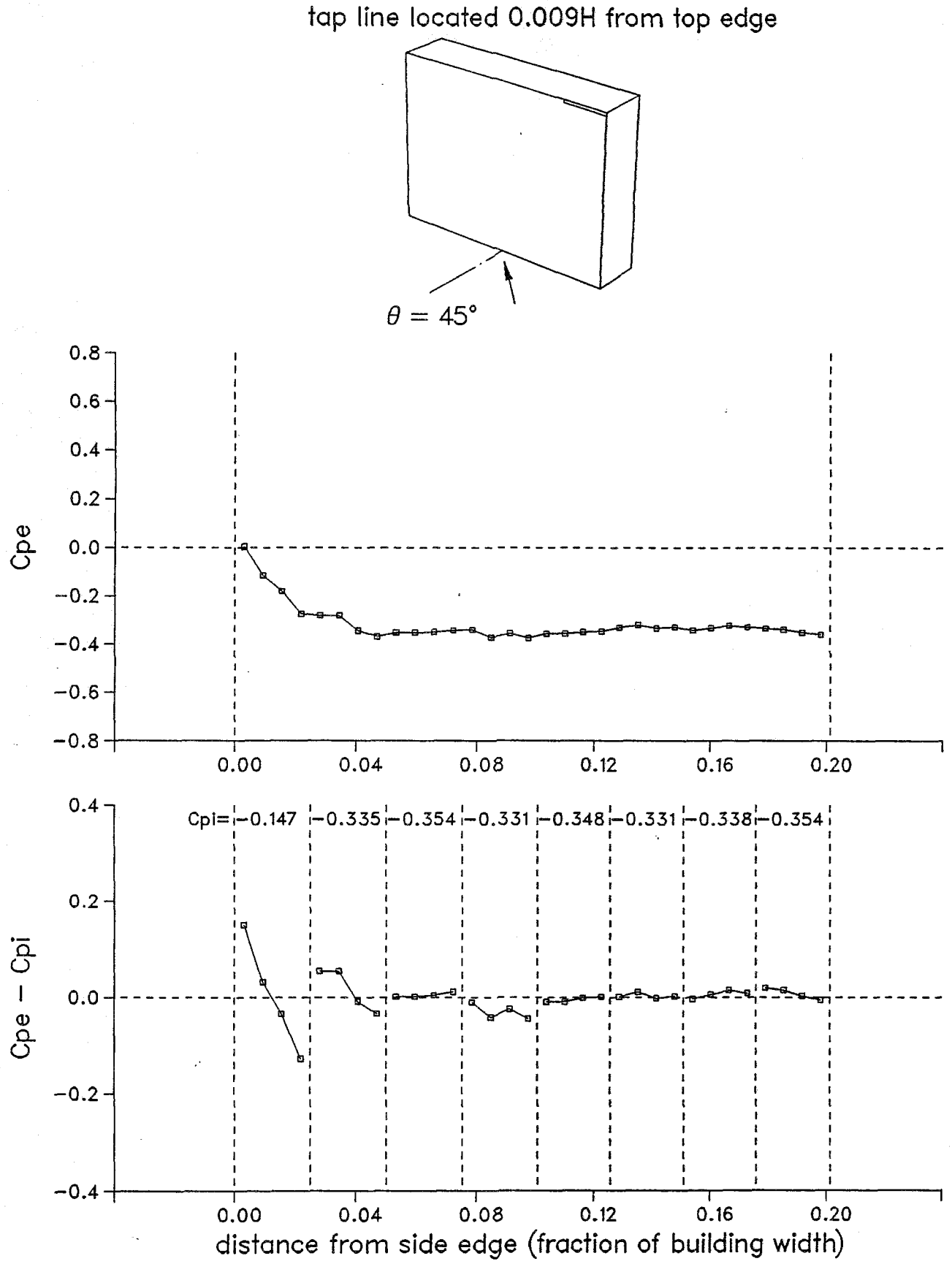

Figure A2.15 Mean pressure distribution on the building surface and the net pressure distribution across the rainscreen with 8 compartments

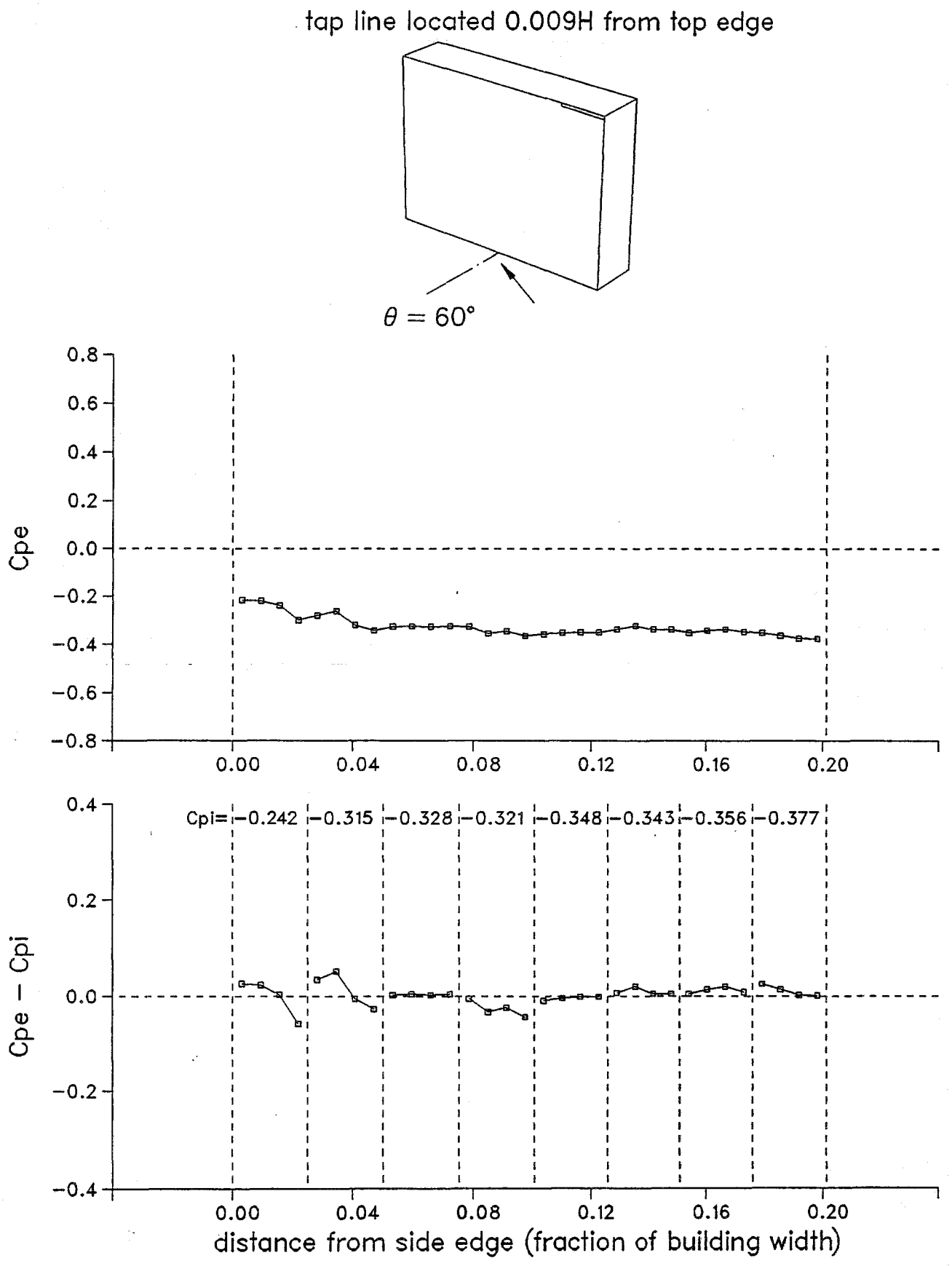

Figure A2.16 Mean pressure distribution on the building surface and the net pressure distribution across the rainscreen with 8 compartments

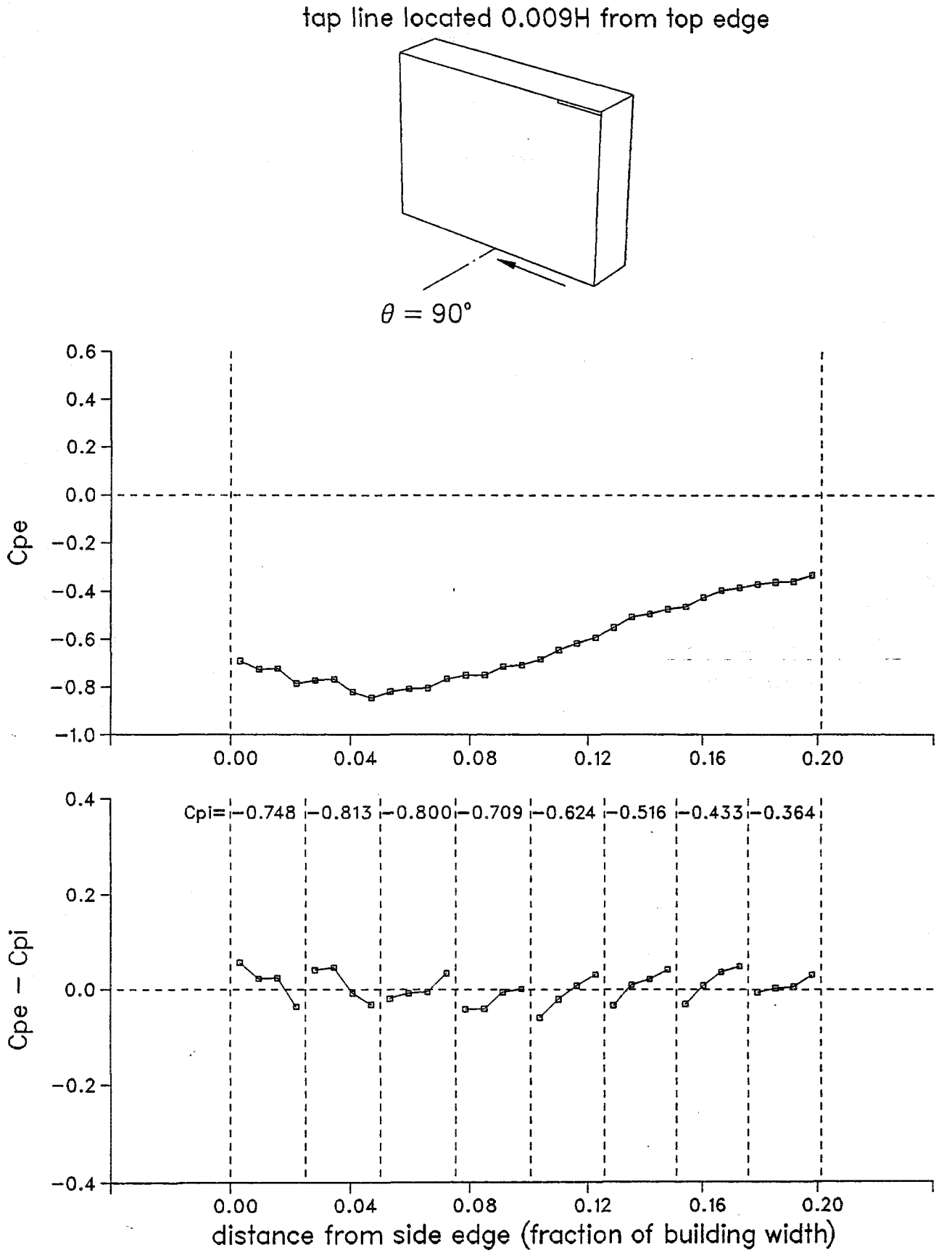

Figure A2.17 Mean pressure distribution on the building surface and the net pressure distribution across the rainscreen with 8 compartments

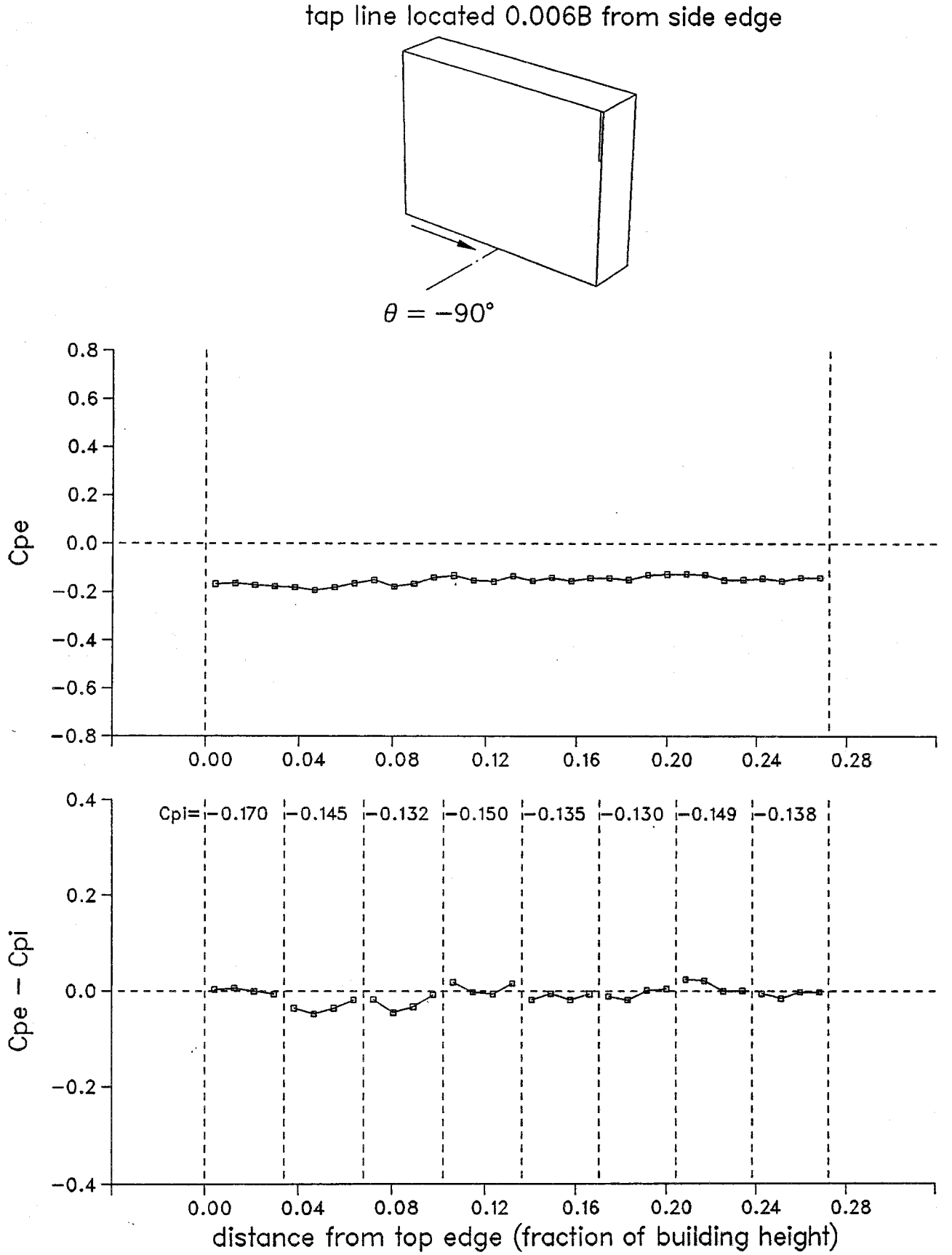

Figure A2.18 Mean pressure distribution on the building surface and the net pressure distribution across the rainscreen with 8 compartments

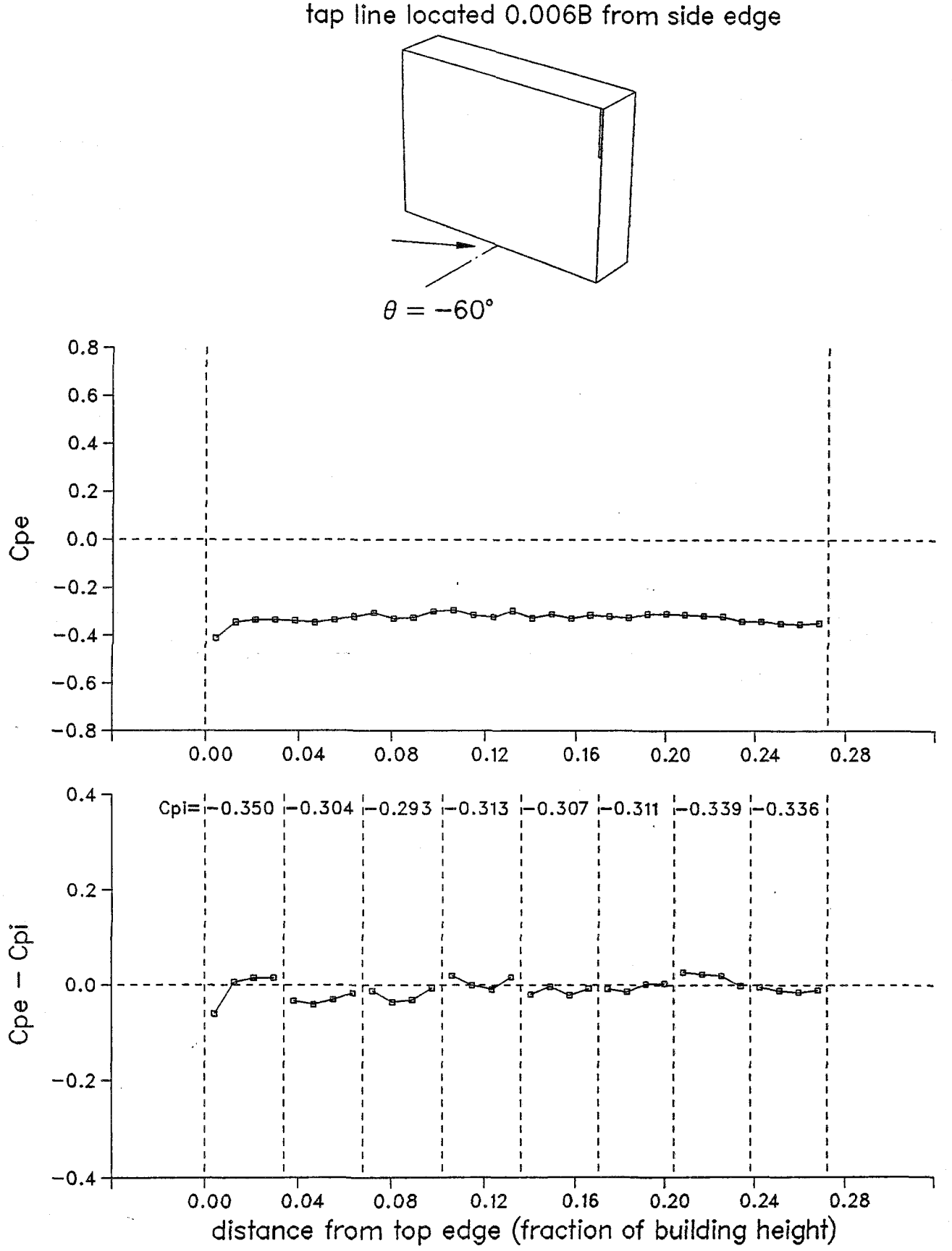

Figure A2.19 Mean pressure distribution on the building surface and the net pressure distribution across the rainscreen with 8 compartments

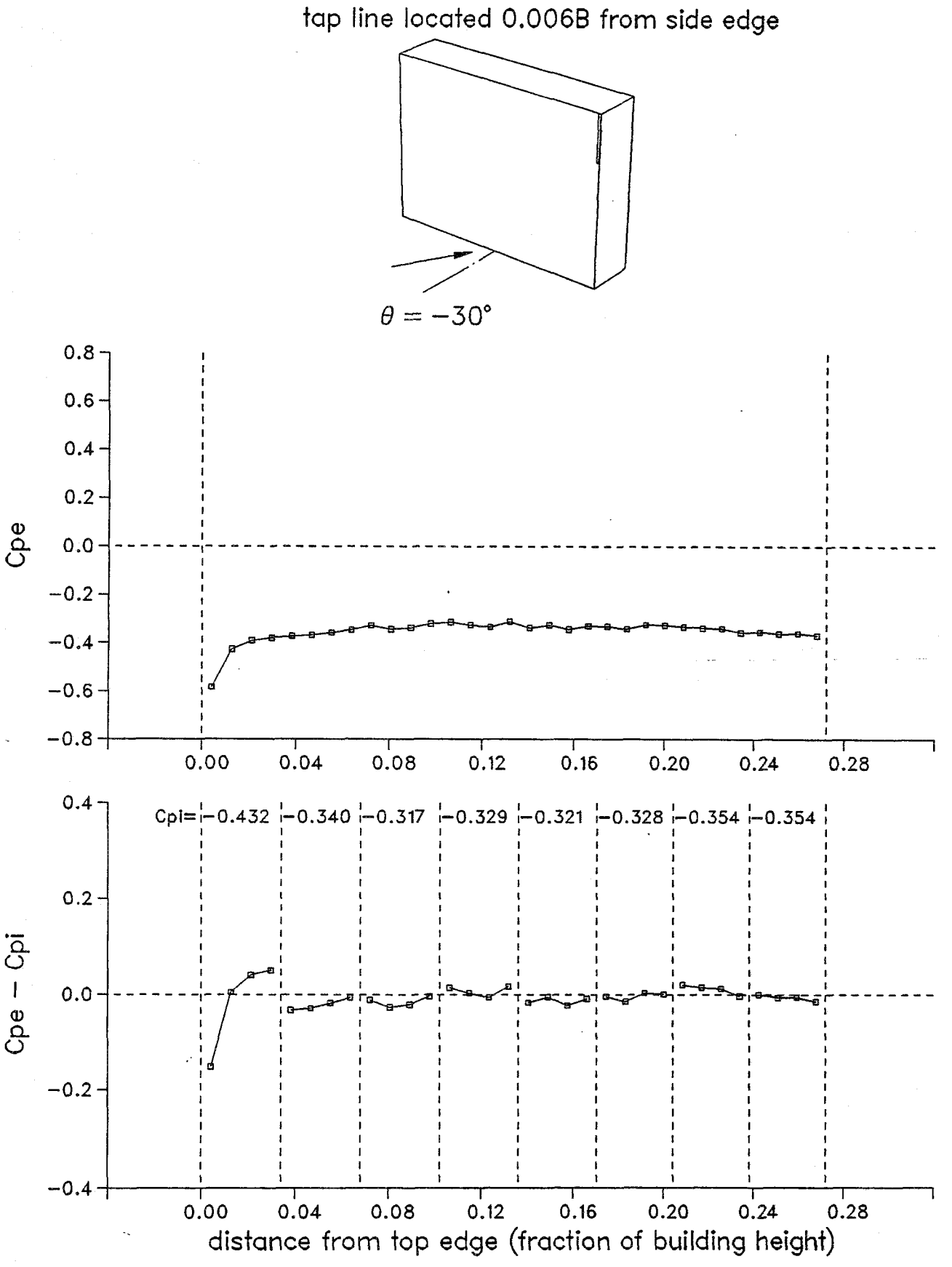

Figure A2.20 Mean pressure distribution on the building surface and the net pressure distribution across the rainscreen with 8 compartments

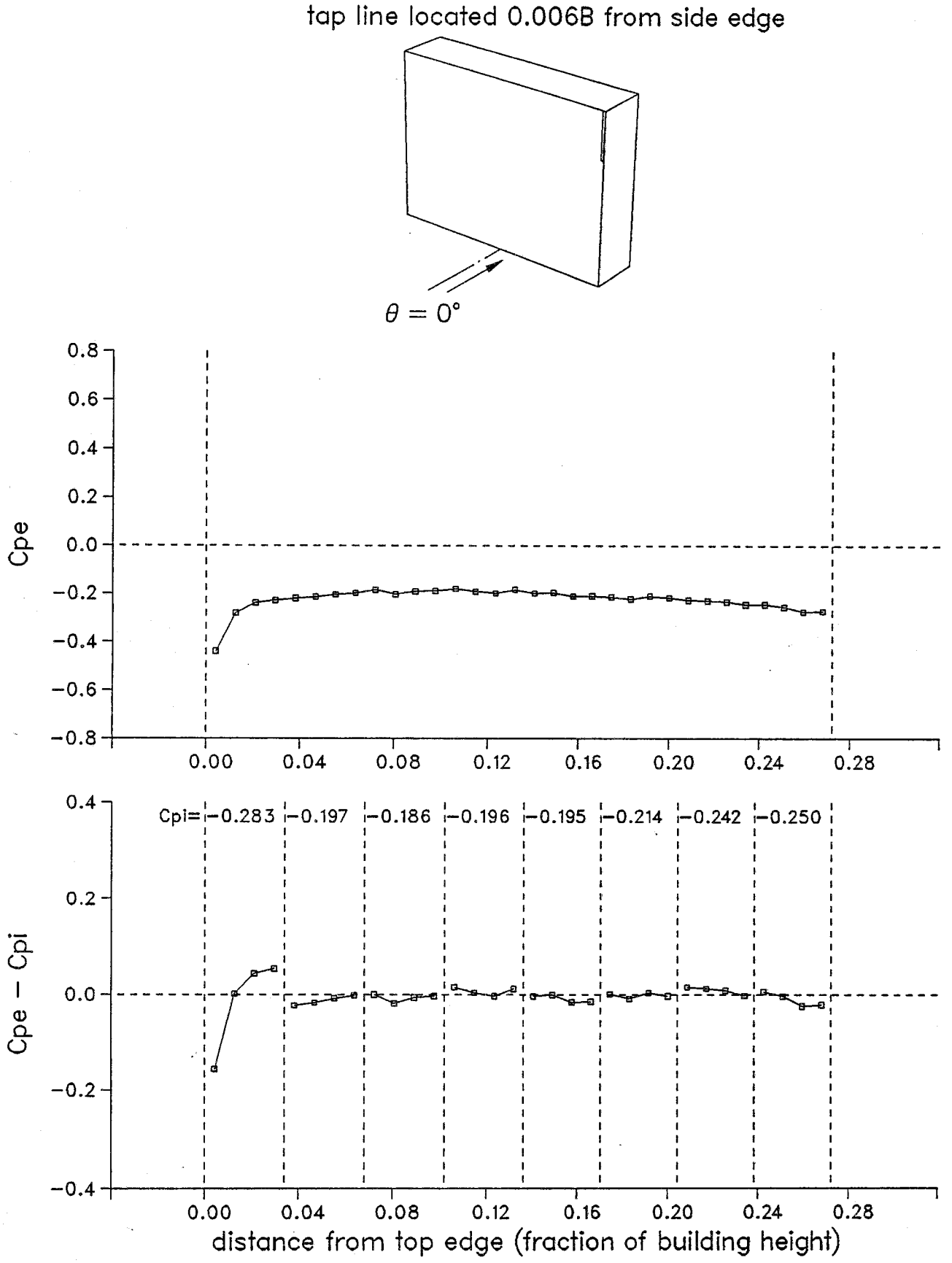

Figure A2.21 Mean pressure distribution on the building surface and the net pressure distribution across the rainscreen with 8 compartments

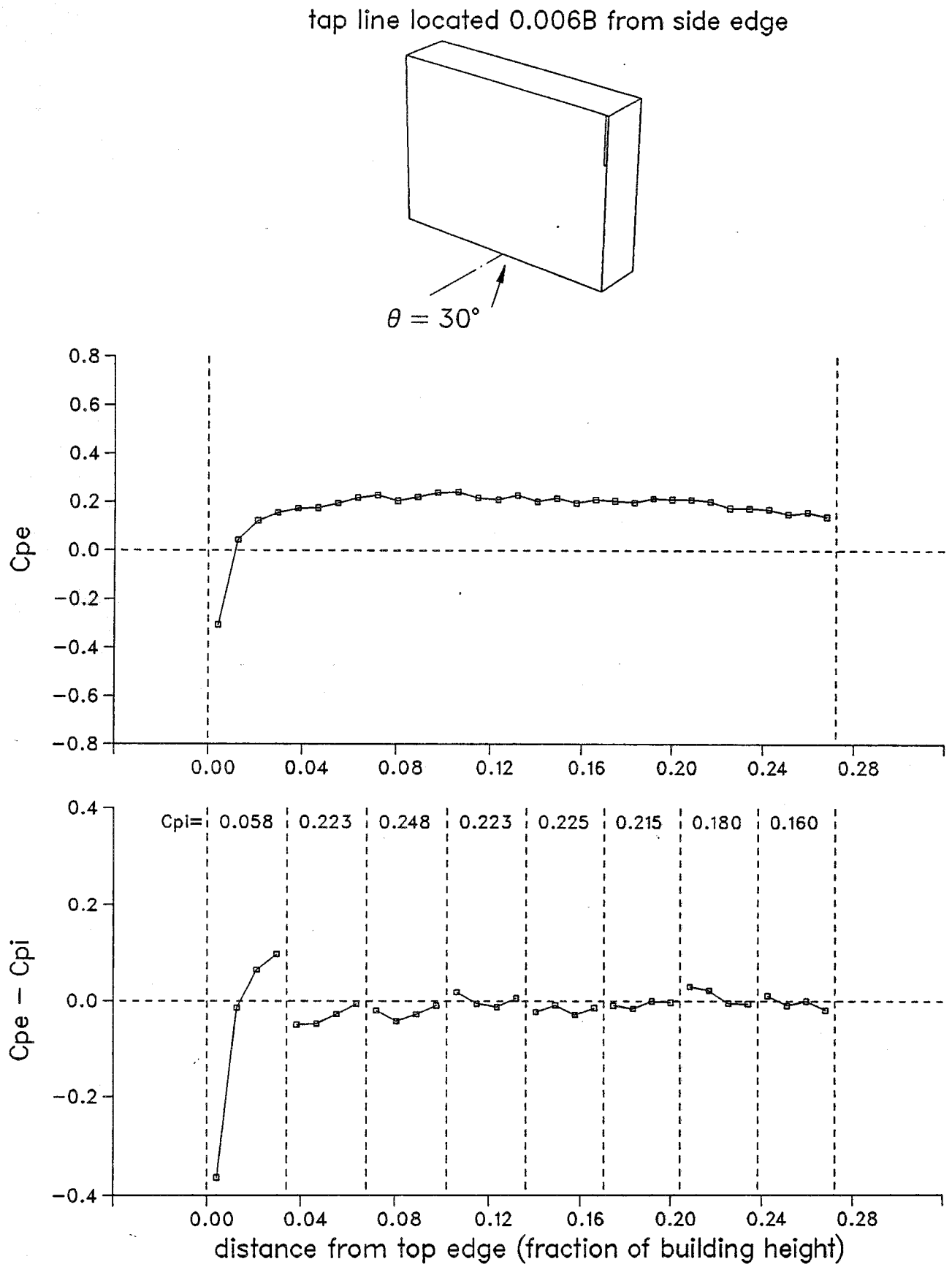

Figure A2.22 Mean pressure distribution on the building surface and the net pressure distribution across the rainscreen with 8 compartments

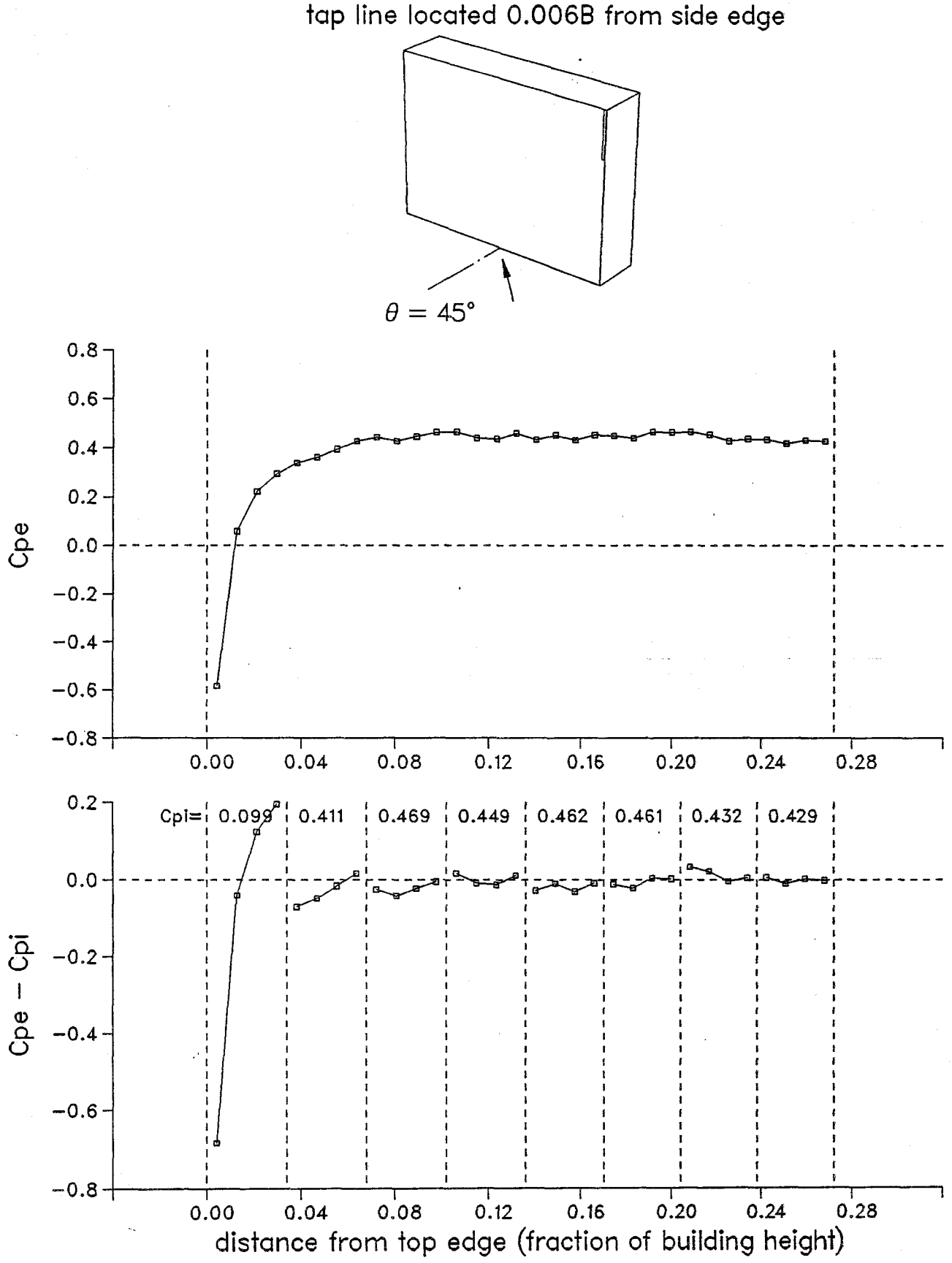

Figure A2.23 Mean pressure distribution on the building surface and the net pressure distribution across the rainscreen with 8 compartments

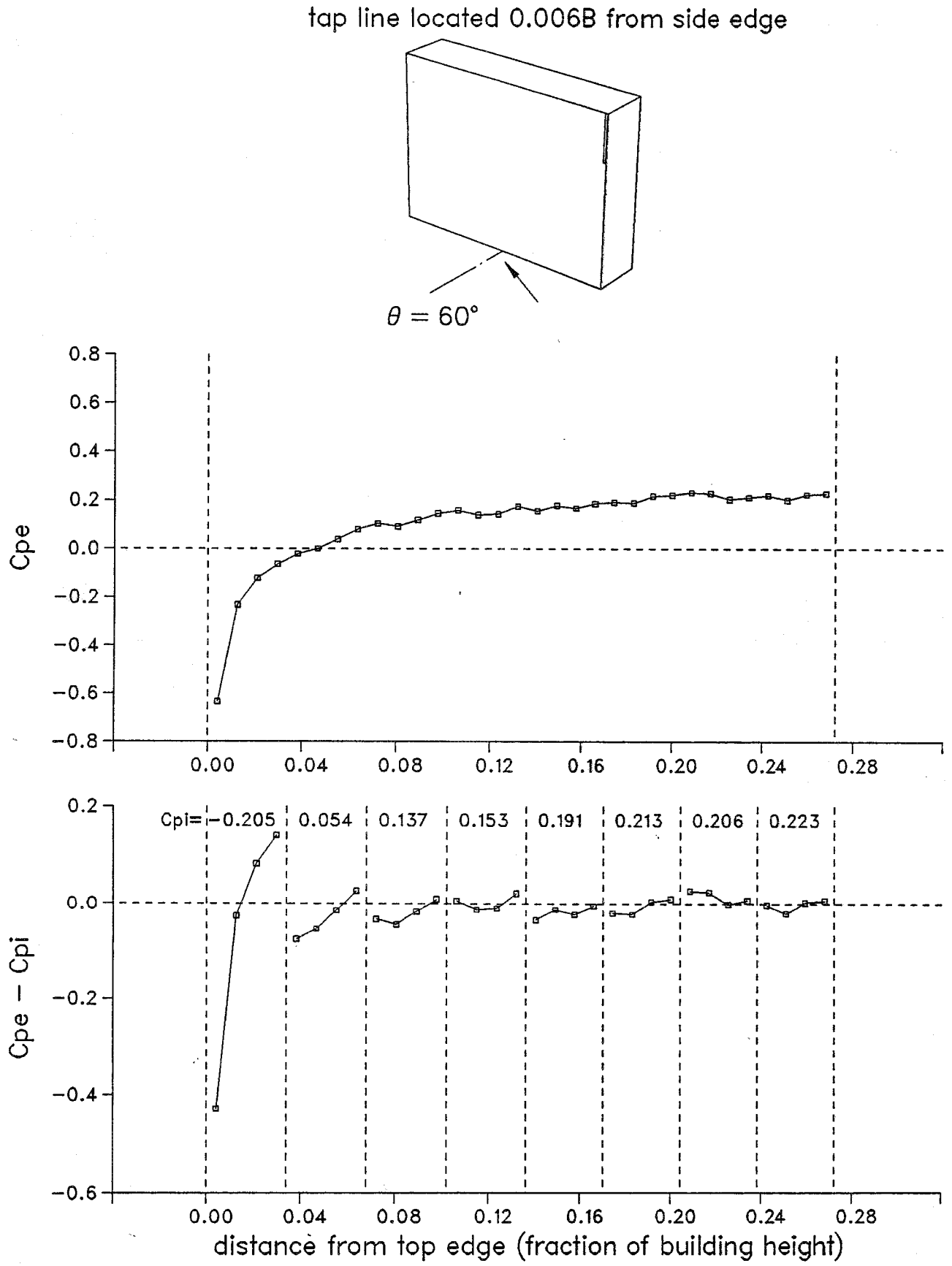

Figure A2.24 Mean pressure distribution on the building surface and the net pressure distribution across the rainscreen with 8 compartments

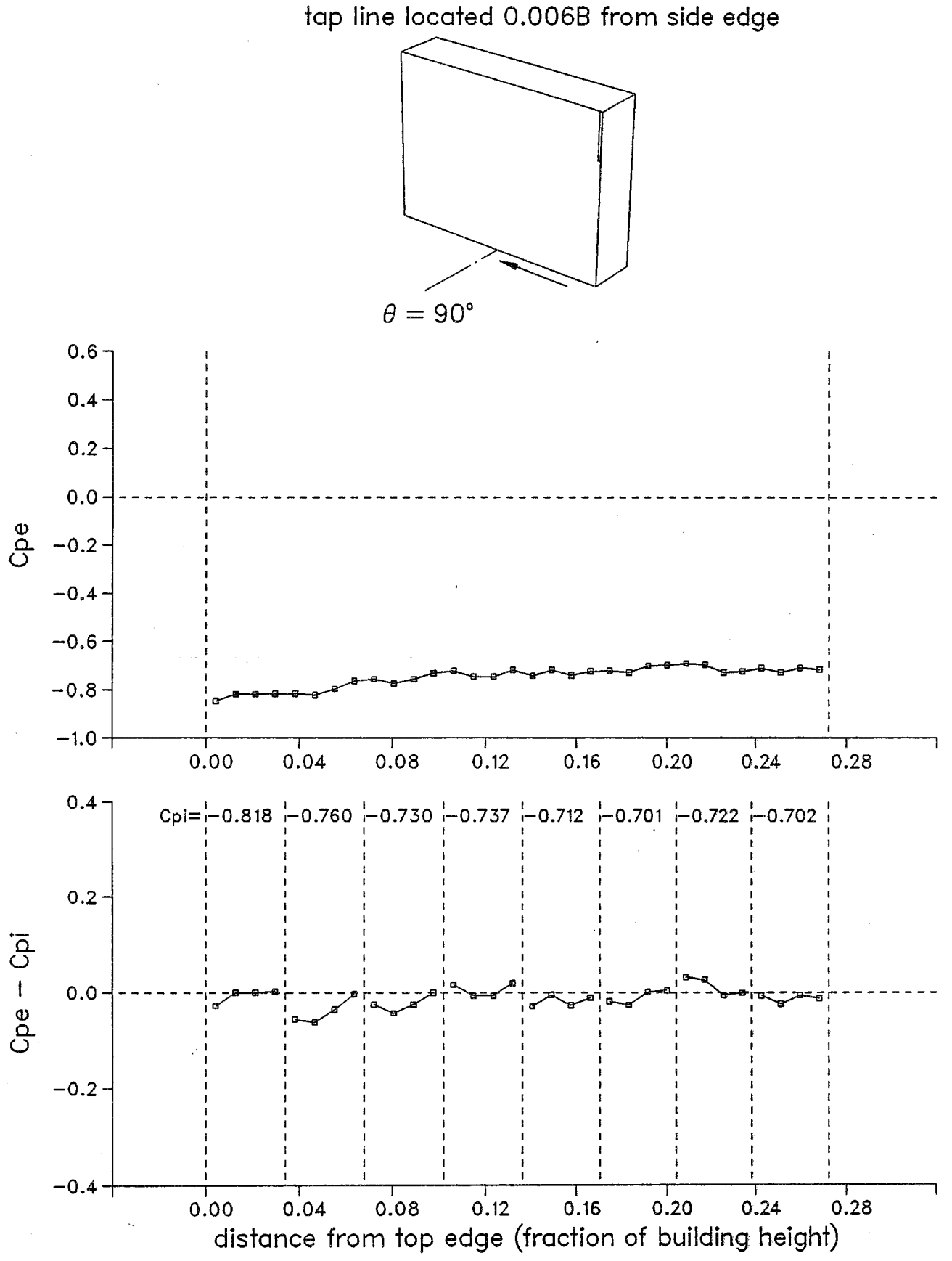

Figure A2.25 Mean pressure distribution on the building surface and the net pressure distribution across the rainscreen with 8 compartments

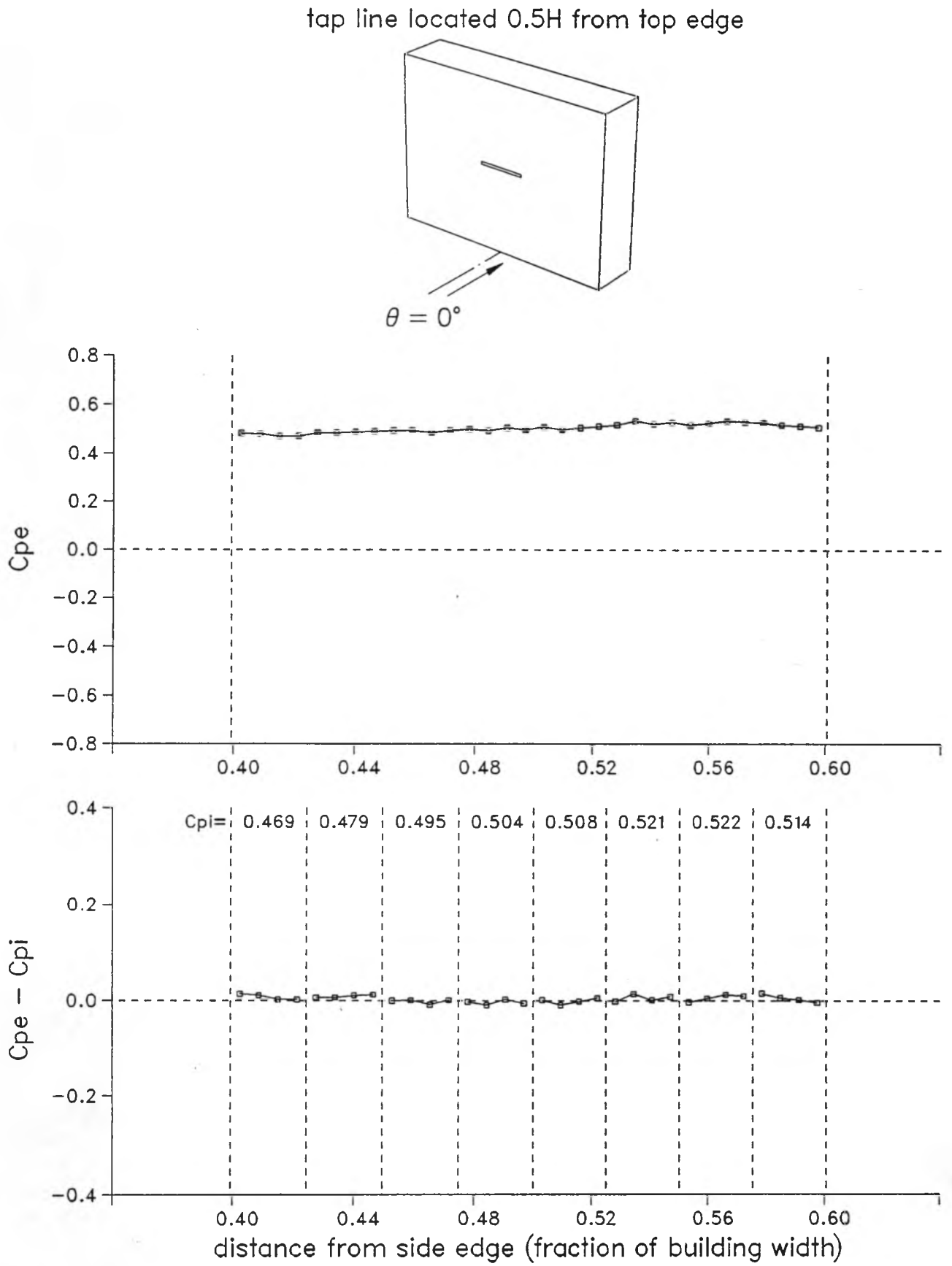

Figure A2.26 Mean pressure distribution on the building surface and the net pressure distribution across the rainscreen with 8 compartments

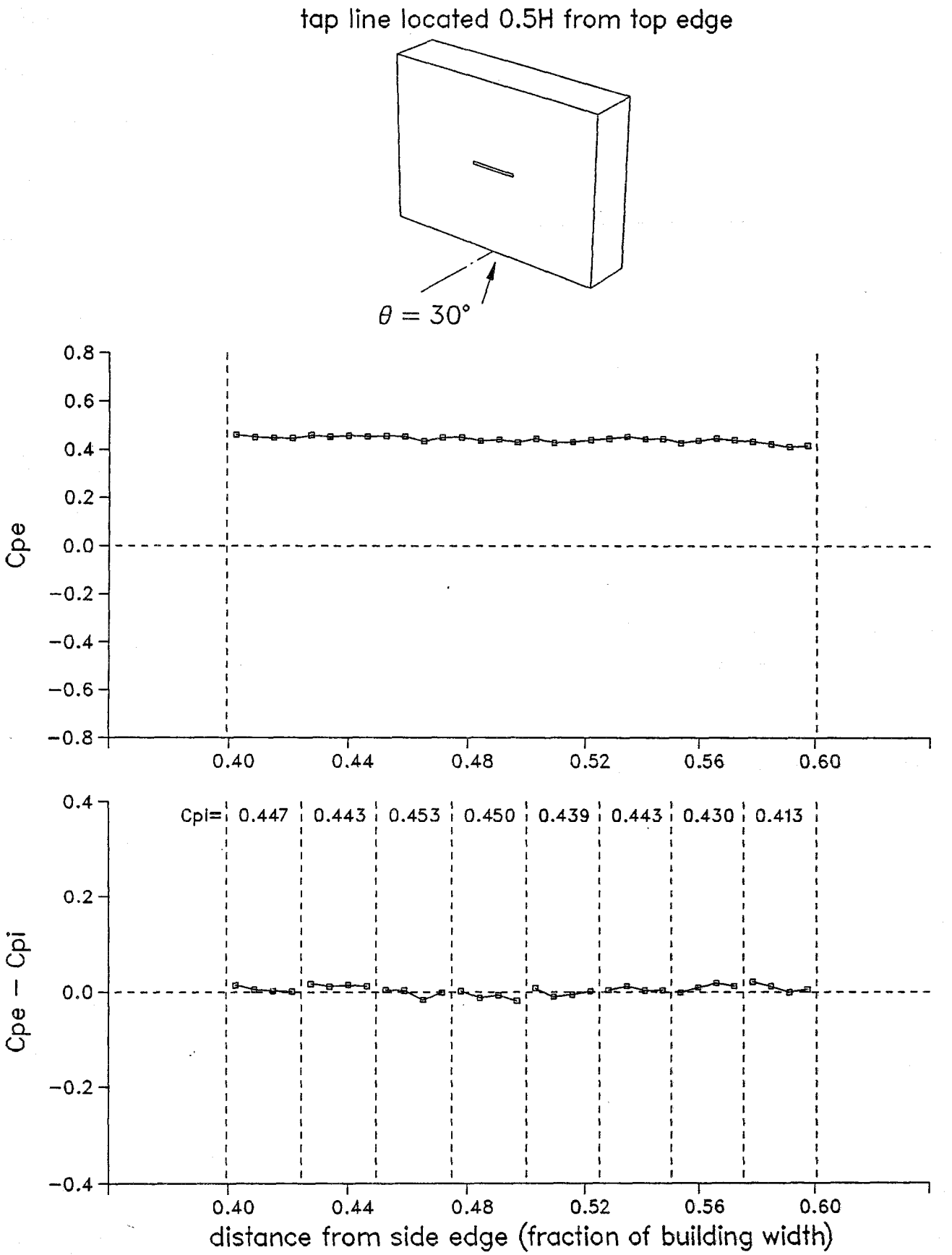

Figure A2.27 Mean pressure distribution on the building surface and the net pressure distribution across the rainscreen with 8 compartments

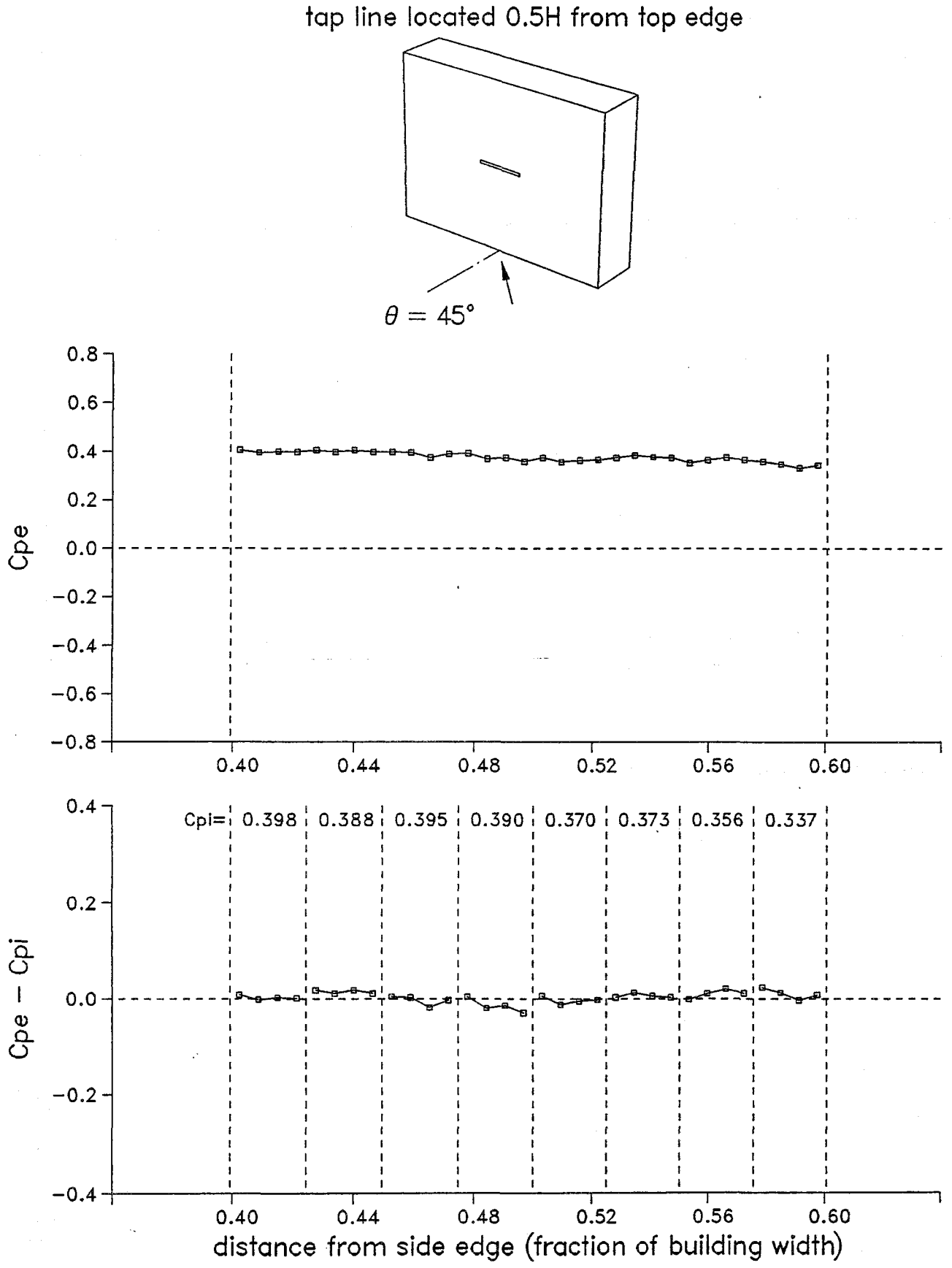

Figure A2.28 Mean pressure distribution on the building surface and the net pressure distribution across the rainscreen with 8 compartments

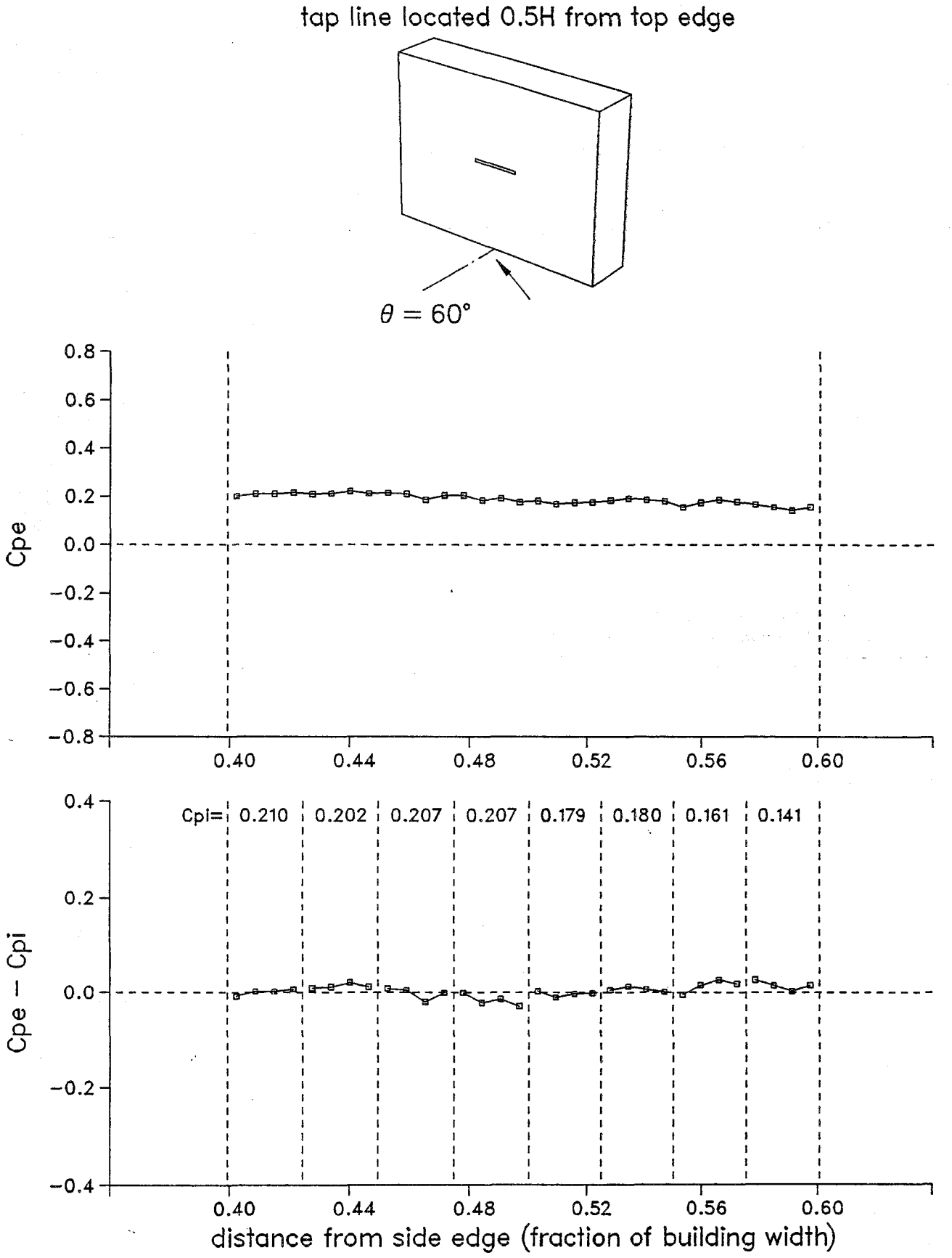

Figure A2.29 Mean pressure distribution on the building surface and the net pressure distribution across the rainscreen with 8 compartments

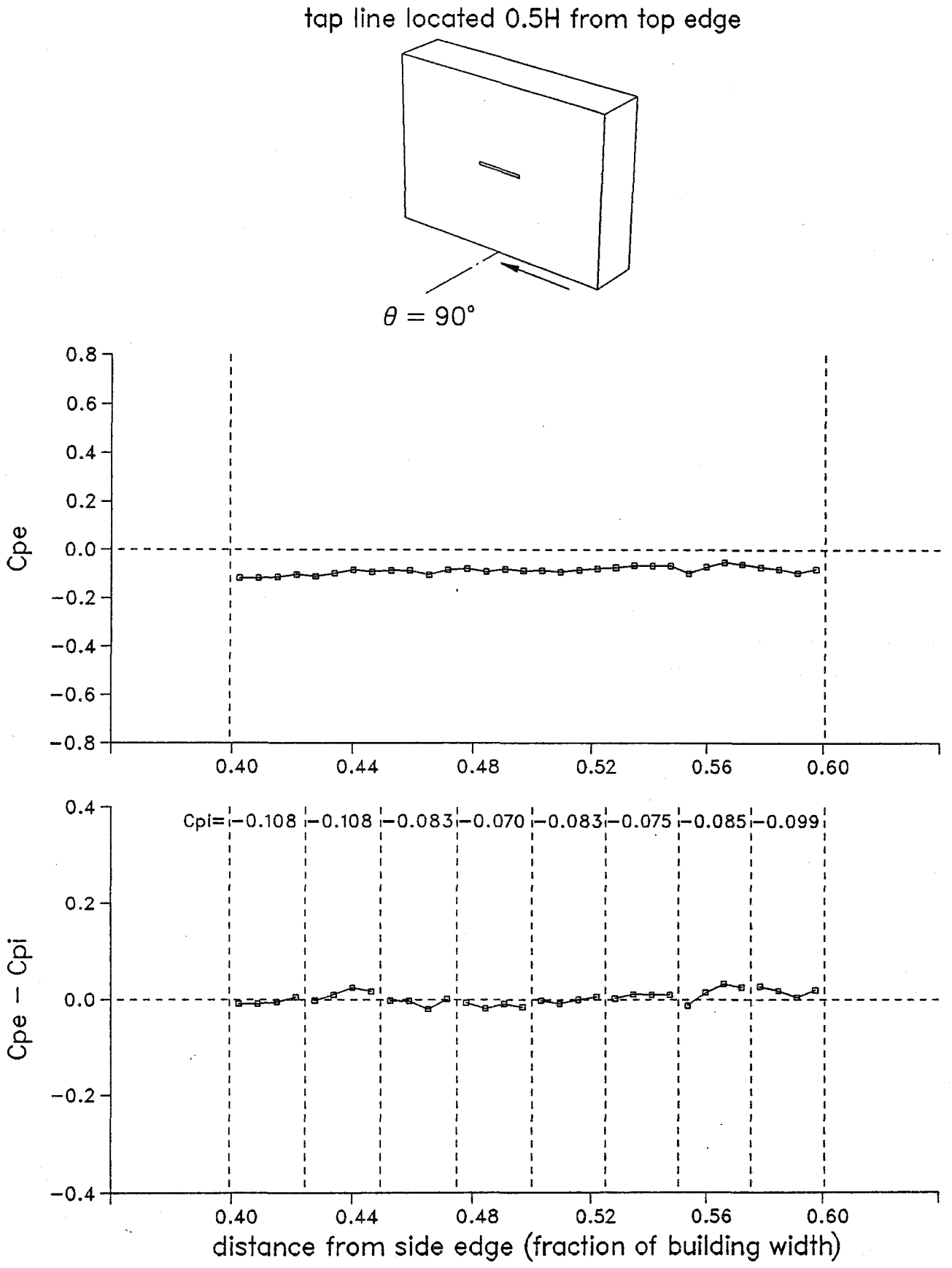

Figure A2.30 Mean pressure distribution on the building surface and the net pressure distribution across the rainscreen with 8 compartments

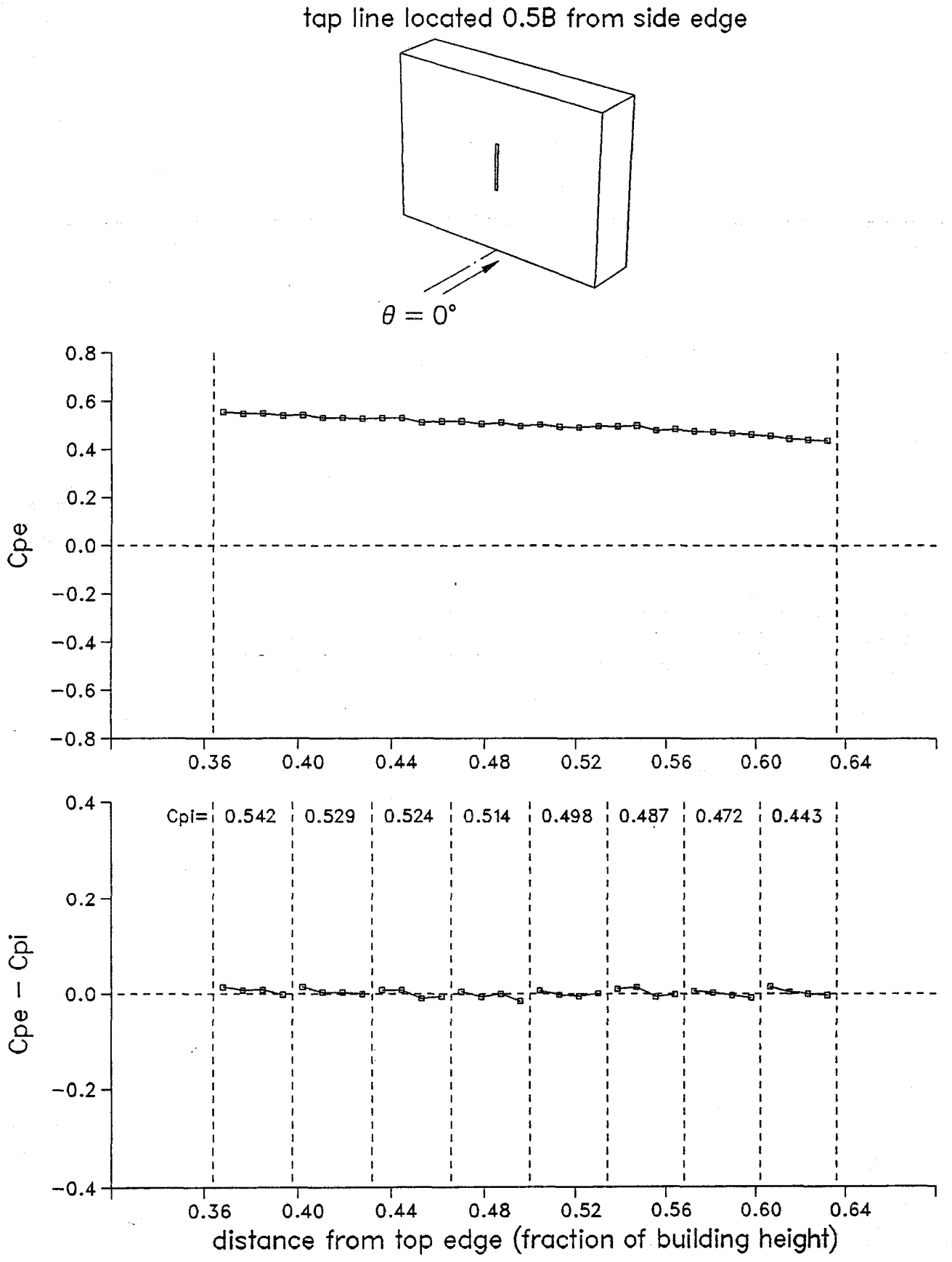

Figure A2.31 Mean pressure distribution on the building surface and the net pressure distribution across the rainscreen with 8 compartments

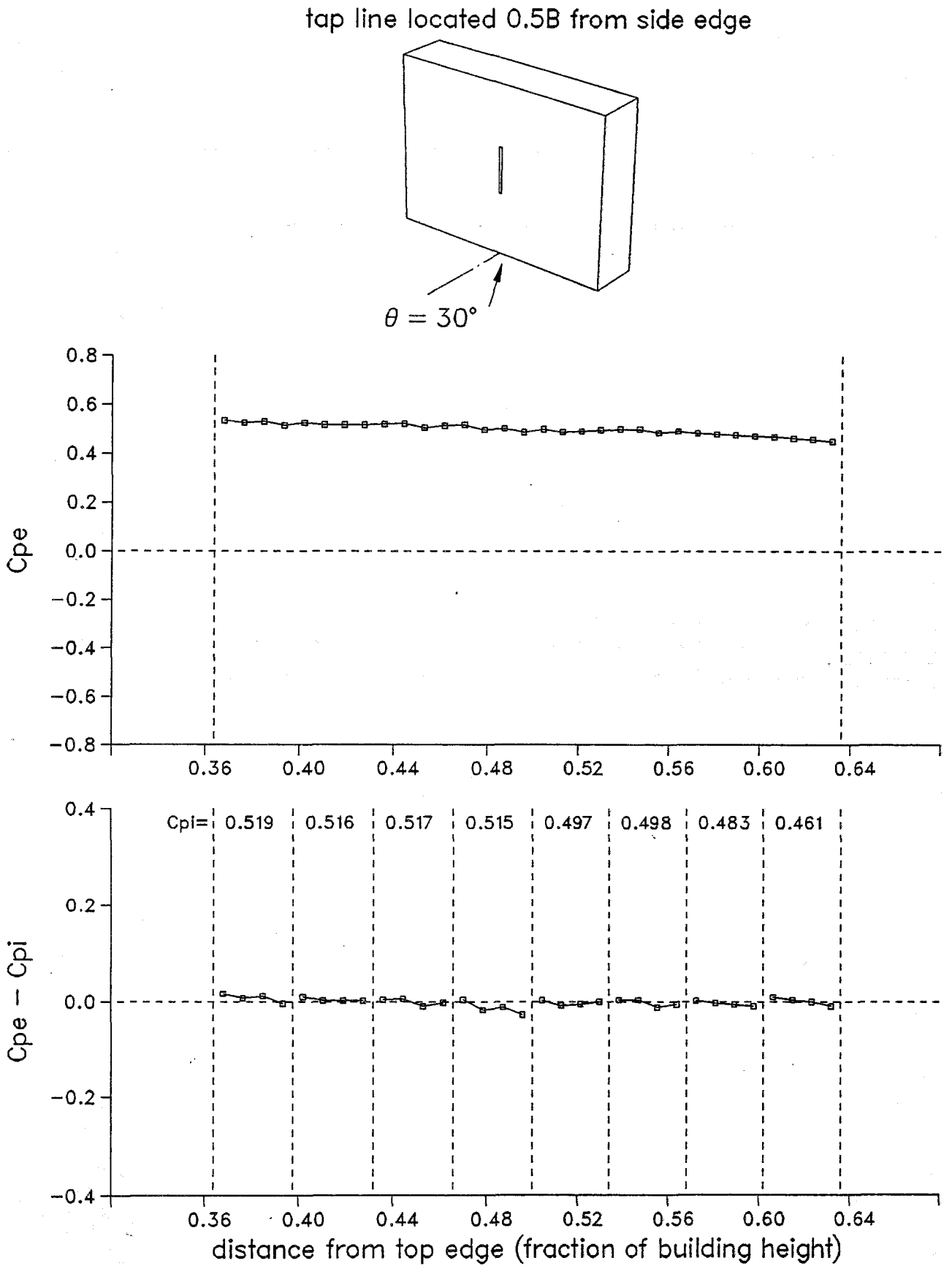

Figure A2.32 Mean pressure distribution on the building surface and the net pressure distribution across the rainscreen with 8 compartments

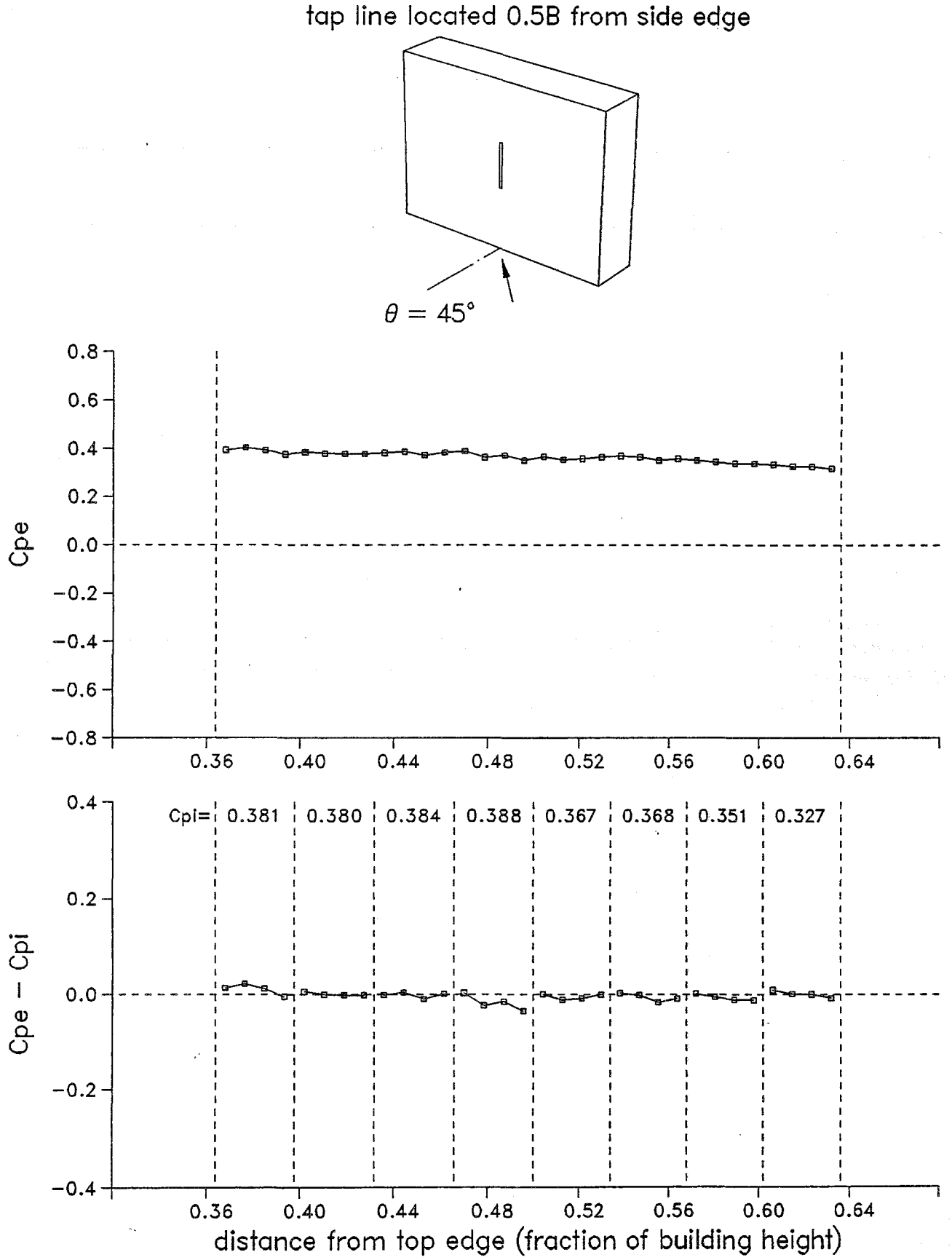

Figure A2.33 Mean pressure distribution on the building surface and the net pressure distribution across the rainscreen with 8 compartments

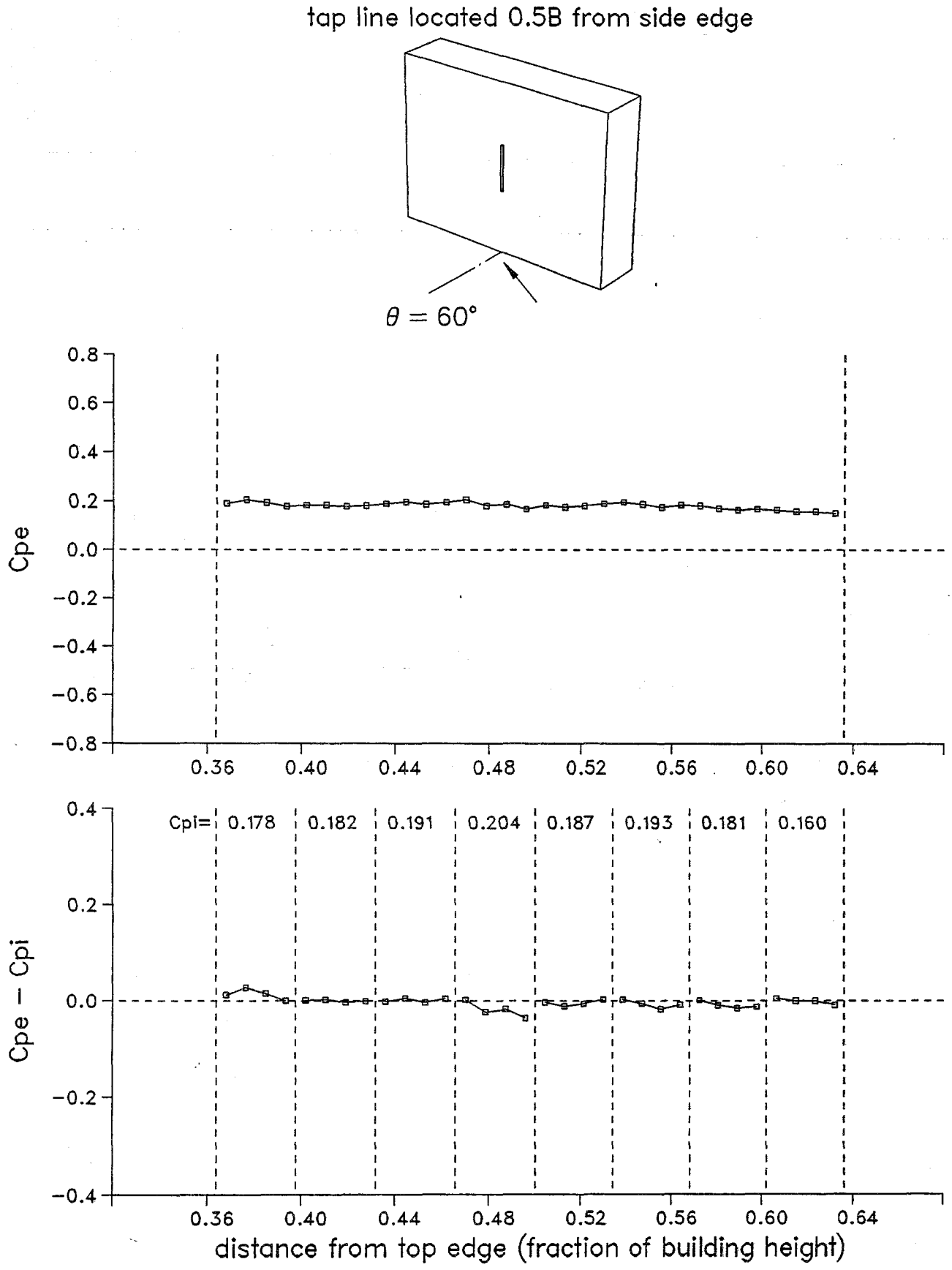

Figure A2.34 Mean pressure distribution on the building surface and the net pressure distribution across the rainscreen with 8 compartments

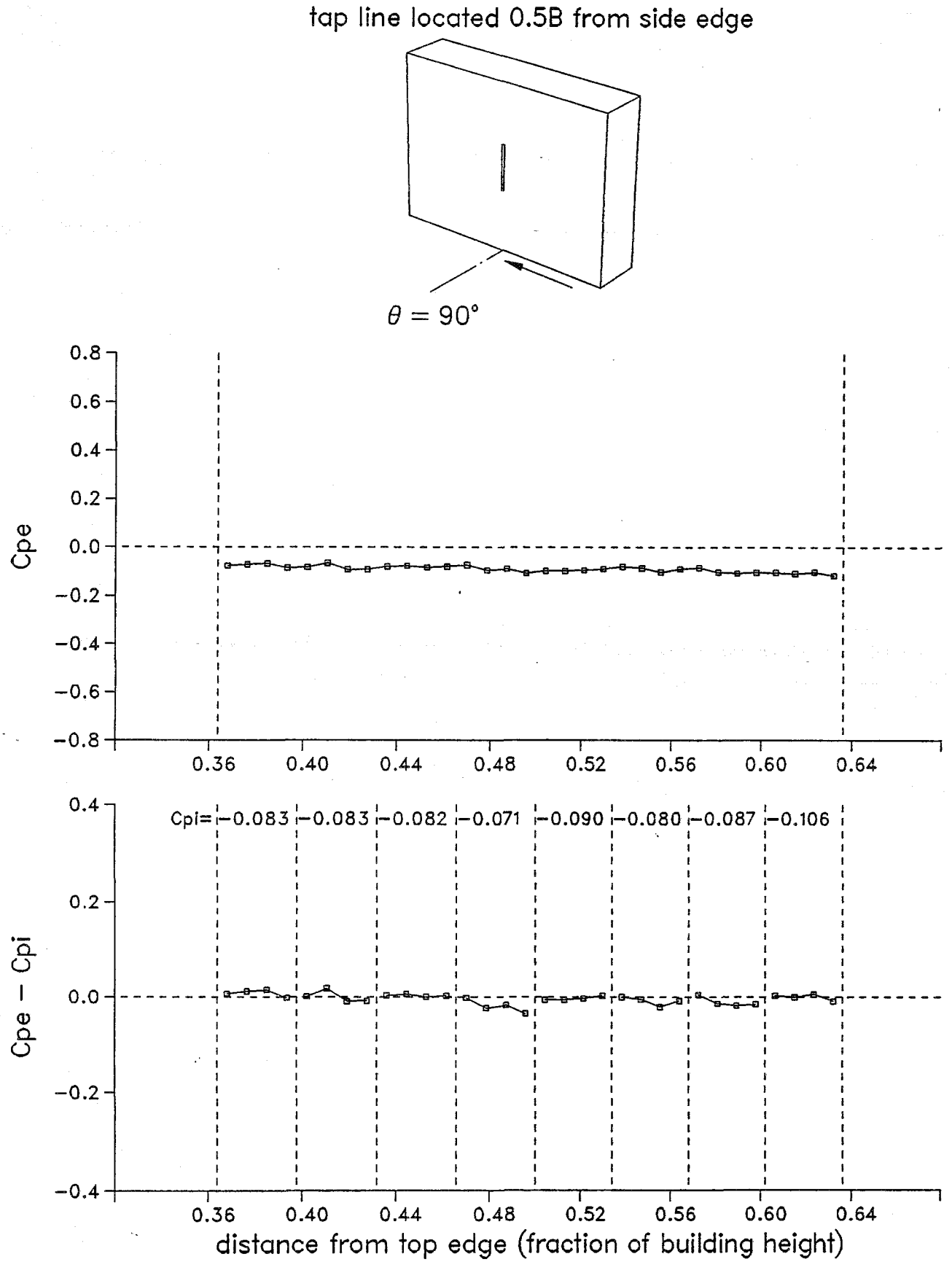

Figure A2.35 Mean pressure distribution on the building surface and the net pressure distribution across the rainscreen with 8 compartments

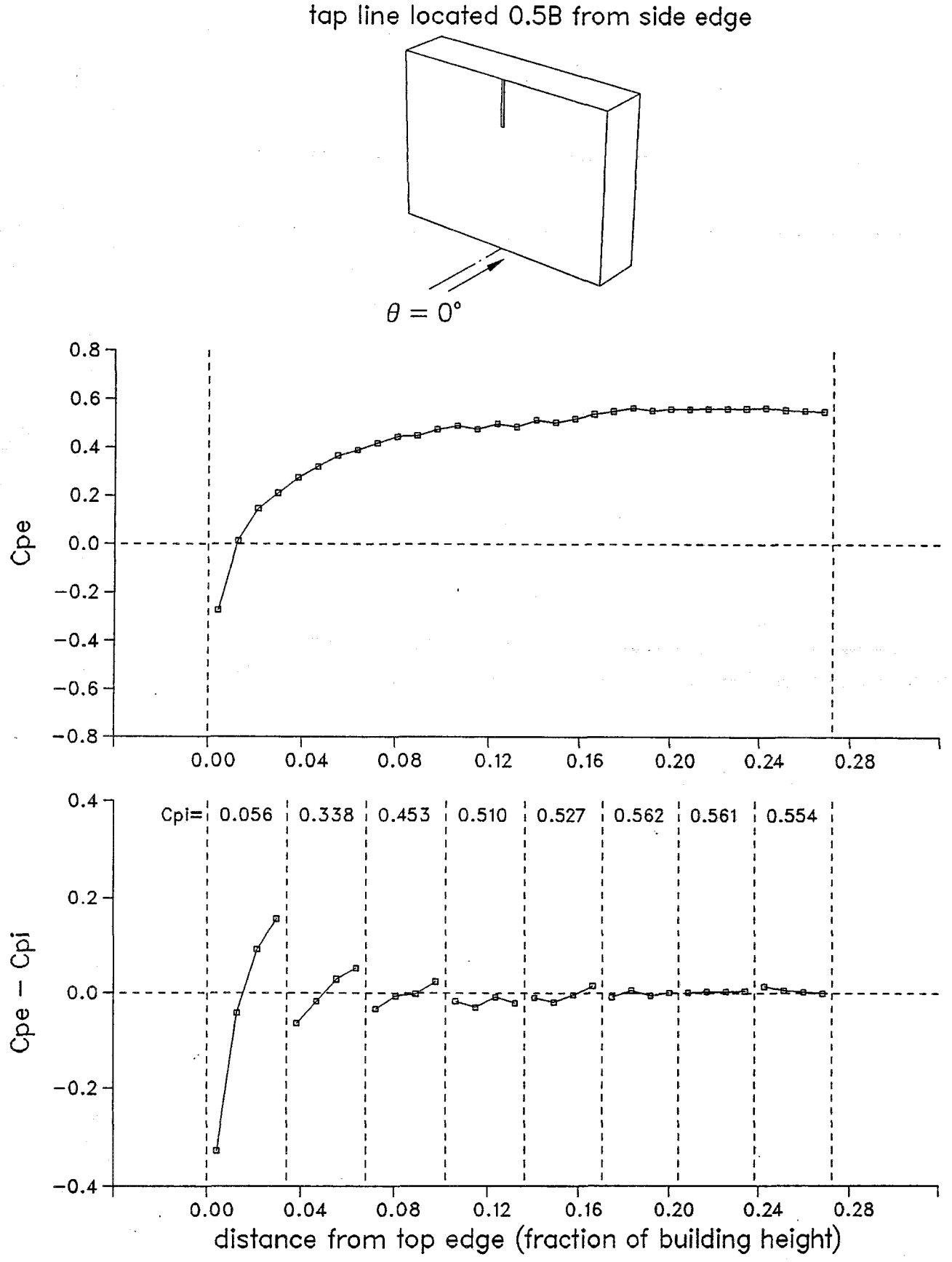

Figure A2.36 Mean pressure distribution on the building surface and the net pressure distribution across the rainscreen with 8 compartments

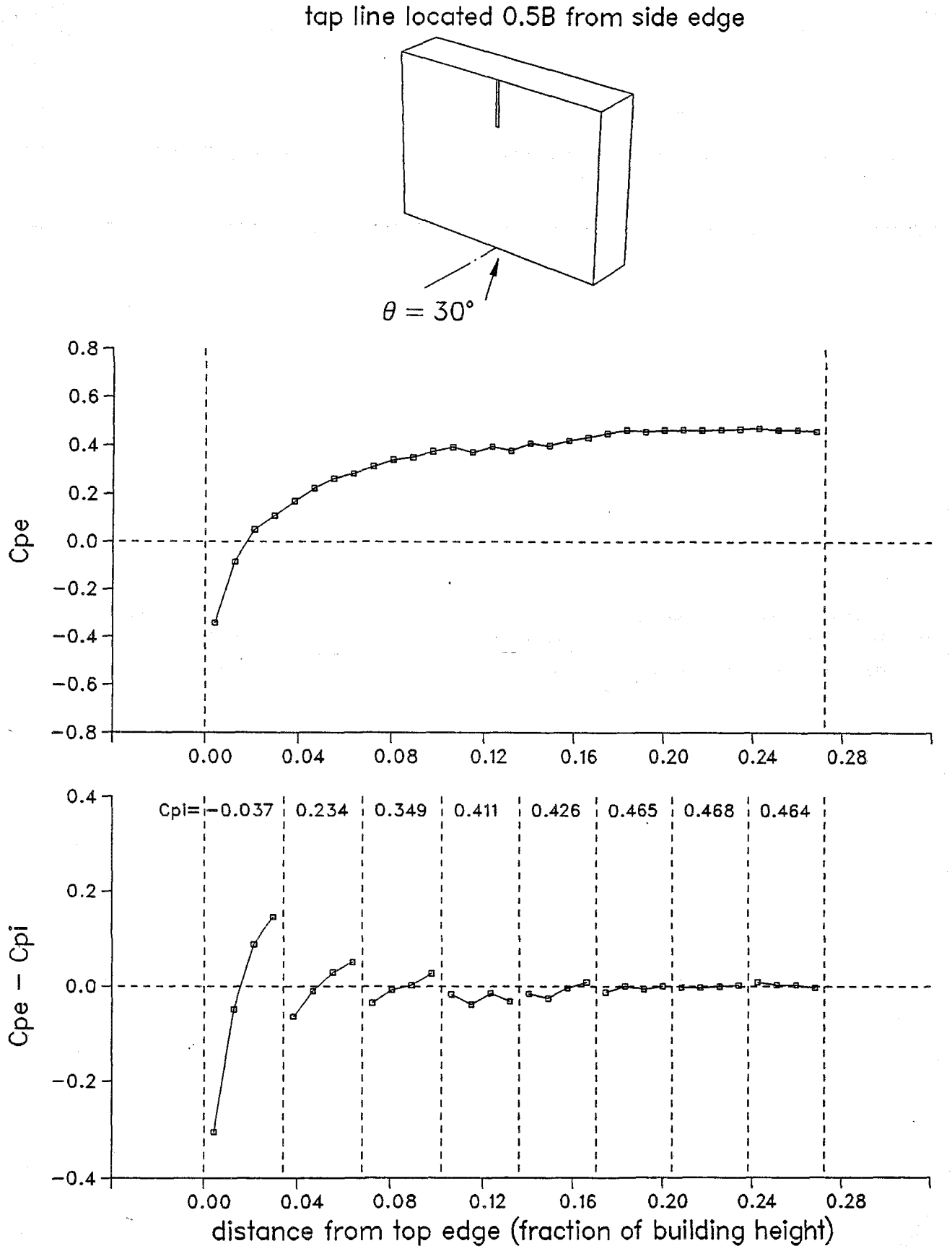

Figure A2.37 Mean pressure distribution on the building surface and the net pressure distribution across the rainscreen with 8 compartments

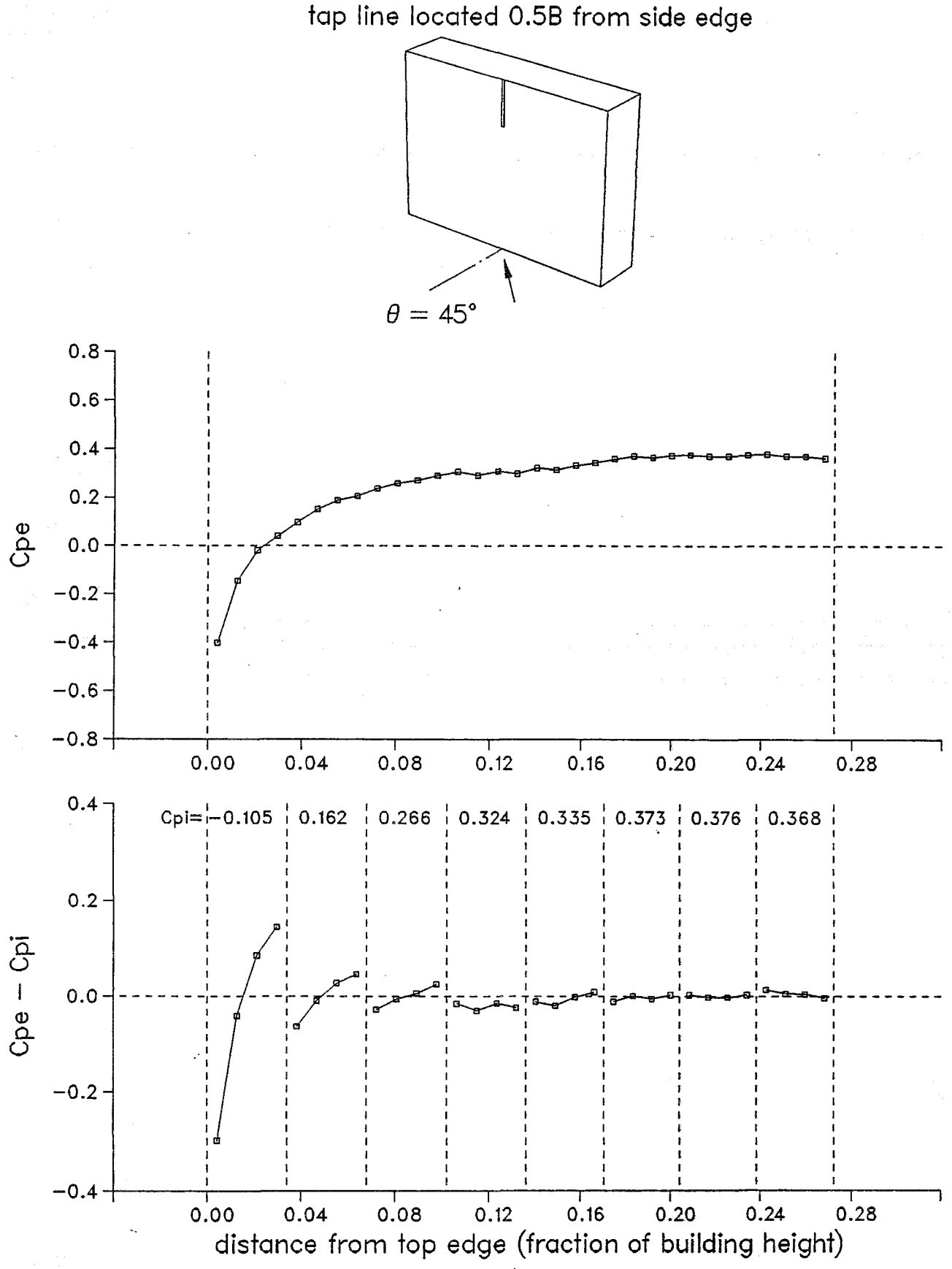

Figure A2.38 Mean pressure distribution on the building surface and the net pressure distribution across the rainscreen with 8 compartments

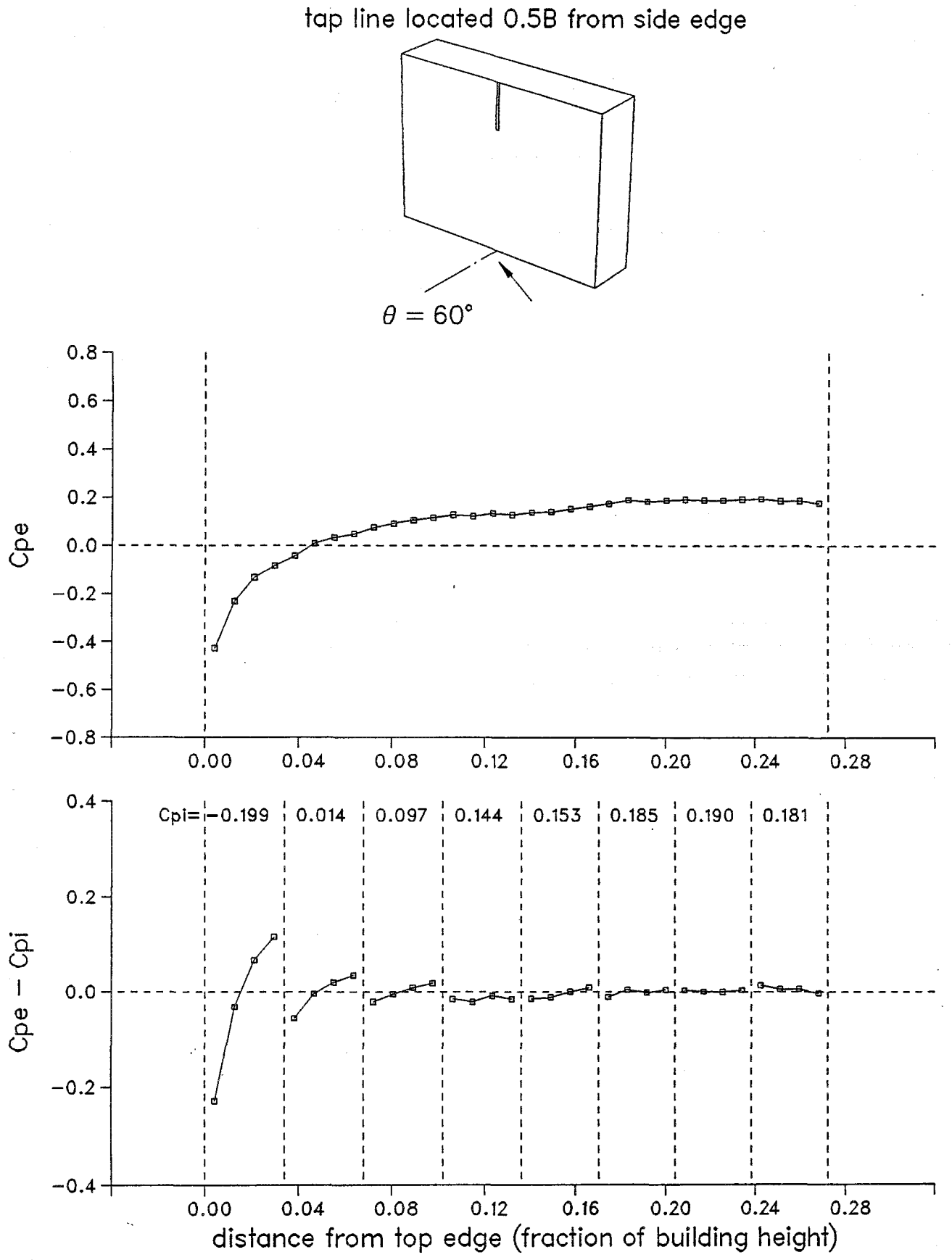

Figure A2.39 Mean pressure distribution on the building surface and the net pressure distribution across the rainscreen with 8 compartments

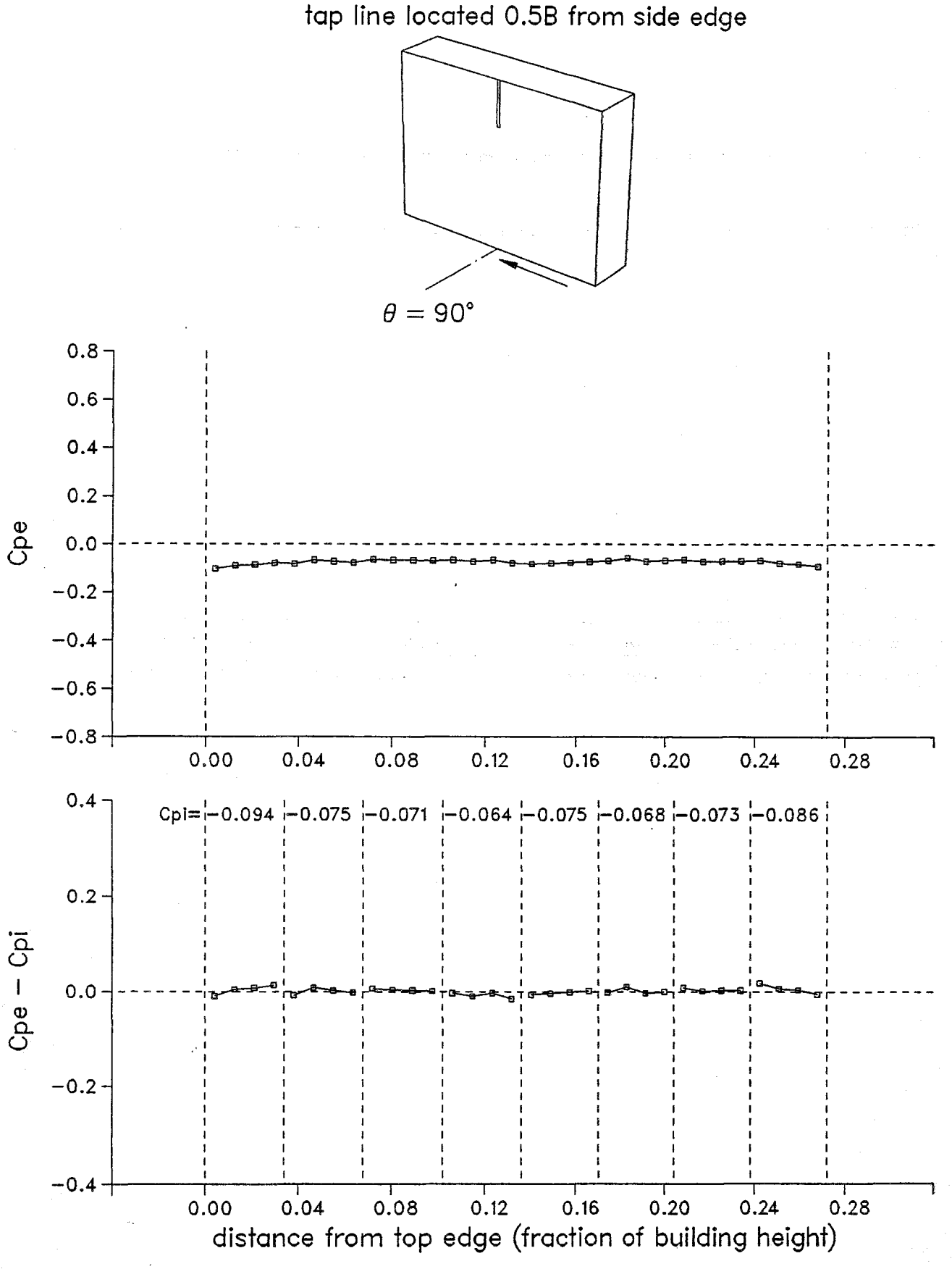

Figure A2.40 Mean pressure distribution on the building surface and the net pressure distribution across the rainscreen with 8 compartments